The VAMP-associated protein VAPB is required for cardiac and neuronal pacemaker channel function

Silbernagel, Nicole; Walecki, Magdalena ; Schafer, Martin K -H; Kessler, Mirjam; Zobeiri, Mehrnoush; Rinné, Susanne; Kiper, Aytug K; Komadowski, Marlene A; Vowinkel, Kirsty S; Wemhoner, Konstantin; Fortmüller, Lisa; Schewe, Marcus ; Dolga, Amalia M; Scekic-Zahirovic, Jelena ; Matschke, Lina A; Culmsee, Carsten; Baukrowitz, Thomas; Monassier, Laurent; Ullrich, Nina D; Dupuis, Luc

The VAMP-associated protein VAPB is required for cardiac and neuronal pacemaker channel function

Nicole Silbernagel,[1] Magdalena Walecki,[1] Martin K.-H. Schäfer,[2] Mirjam Kessler,[3] Mehrnoush Zobeiri,[4] Susanne Rinné,[1] Aytug K. Kiper,[1] Marlene A. Komadowski,[1,2] Kirsty S. Vowinkel,[1] Konstantin Wemhöner,[1] Lisa Fortmüller,[5] Marcus Schewe,[10] Amalia M. Dolga,[11] Jelena Scekic-Zahirovic,[6] Lina A. Matschke,[1] Carsten Culmsee,[11] Thomas Baukrowitz,[10] Laurent Monassier,[6] Nina D. Ullrich,[12] Luc Dupuis,[7,8] Steffen Just,[3] Thomas Budde,[4] Larissa Fabritz,[5,9] and Niels Decher[1,*]

[1]Institute of Physiology and Pathophysiology, Vegetative Physiology, Phillips University, Marburg 35037, Germany; [2]Institute of Anatomy and Cell Biology, Philipps University, Marburg 35037, Germany; [3]Molecular Cardiology, Department of Internal Medicine II, University Hospital Ulm, Ulm 89081, Germany; [4]Institute for Physiology I, University of Münster, Münster 48149, Germany; [5]Department of Cardiovascular Medicine, University Hospital Münster, Münster 48149, Germany; [6]Inserm U1118, Mécanismes centraux et périphériques de la neurodegenerescence, Faculté de médecine, Université de Strasbourg, Strasbourg 67000, France; [7]Laboratoire de Neurobiologie et Pharmacologie Cardiovasculaire, Faculté de Médecine Strasbourg, Strasbourg 67000, France; [8]INSERM, faculté de médecine, Université de Strasbourg, Strasbourg 67000, France; [9]Institute of Cardiovascular Sciences, University of Birmingham and Department of Cardiology, University Hospital Birmingham, Birmingham B15 2TT, United Kingdom and Division of Rhythmology, University Hospital Münster, Münster 48149, Germany; [10]Institute of Physiology, Christian-Albrechts University, Kiel 24118, Germany; [11]Institute of Pharmacology and Clinical Pharmacy, Phillips University, Marburg 35032, Germany; [12]Institute of Physiology und Pathophysiology, University of Heidelberg, Heidelberg 69120, Germany

*Correspondence to:
Prof. Dr. Niels Decher
Philipps-Universität Marburg
Institut für Physiologie und Pathophysiologie, Vegetative Physiologie
Deutschhausstraße 1-2
D-35037 Marburg, Germany
E-mail: decher@staff.uni-marburg.de
Phone: +49-6421-28-62148
Fax: +49-6421-28-66659

Running title: VAPB a novel HCN channel subunit

ABBREVATIONS:

ALS, amyotrophic lateral sclerosis; CNBD, cyclic nucleotide-binding domain; Dig, Digoxigenin; HA, hemagglutinin; HCN channels, Hyperpolarization-activated cyclic-nucleotide-gated channels; hpf, hours post fertilization; IML, intermediolateral nucleus; ISH, in-situ hybridization; MO, Morpholino-modified antisense oligonucleotides; Pir, piriform cortex; RTh, reticular thalamic nucleus; Sth, subthalamic nucleus; TC, thalamocortical neurons; TEVC, Two-electrode voltage-clamp; VAMP, vesicle-associated membrane protein; VAPB, VAMP-Associated Protein B; VB, ventrobasal thalamic complex; Y2H, Yeast Two-Hybrid

ABSTRACT: Hyperpolarization-activated cyclic-nucleotide-gated (HCN) channels encode neuronal and cardiac pacemaker currents. The composition of pacemaker channel complexes in different tissues is poorly understood and the presence of additional HCN modulating subunits was speculated. Here we show that VAMP-Associated Protein B (VAPB), previously associated with a familial form of amyotrophic lateral sclerosis 8 (ALS8), is an essential HCN1 and HCN2 modulator. VAPB significantly increases HCN2 currents and surface expression and has a major influence on the dendritic neuronal distribution of HCN2. Severe cardiac bradycardias in VAPB-deficient zebrafish and VAPB$^{-/-}$ mice highlight that VAPB physiologically serves to increase cardiac pacemaker currents. An altered T-wave morphology observed in ECGs of VAPB$^{-/-}$ mice supports the recently proposed role of HCN channels for ventricular repolarization. The critical function of VAPB in native pacemaker channel complexes will be relevant for our understanding of cardiac arrhythmias, epilepsies, and provides an unexpected link between these diseases and ALS.

KEY WORDS: HCN channels · VAPB · ALS · pacemaker · cardiac arrhythmia

INTRODUCTION

Hyperpolarization-activated cyclic-nucleotide gated (HCN) channels play a major role in generating neuronal and cardiac automaticity (1). Upon hyperpolarization HCN channels induce an unspecific cationic conductance, mediated by Na^+ and K^+ (2), described as I_h and I_q in the brain or I_f in the heart. These pacemaker currents regulate the heart rate (3), as well as rhythmic activity in neuronal circuits (4, 5) and synaptic transmission (6), but are also important for setting the resting membrane potential (7). The conserved cyclic-nucleotide-binding-domain (CNBD) in the C-terminus of HCN channels (8) confers a cAMP-sensitivity to the channels (9, 10) which can be antagonized by an allosteric competition with the auxiliary HCN subunit Trip8b (11, 12). However, remaining differences in voltage-dependence and pharmacology of pacemaker currents in native tissues towards the four known HCN channels suggest the presence of additional HCN channel modulating proteins.

Here, we describe a novel interaction partner and modulator of HCN1 and HCN2, the vesicle-associated membrane protein (VAMP)-associated protein B (VAPB or ERG30) (13). VAPs were initially described as interacting partners of VAMP, participating in neurotransmitter release (14). VAPs are, in addition to the ER, found in many intracellular compartments including i.e. the Golgi apparatus, recycling endosomes, tight junctions, but also the plasma membrane (15, 16). Both family members, VAPA (VAP-33) (17) and VAPB form a complex via their transmembrane domains and are part of the vSNARE complex (16). It has been proposed that VAPB is not directly participating in synaptic vesicle exocytosis, but rather in the targeting of components to the synaptic terminals (18). In addition, previous studies of Kv2.1 and VAMP (19), TASK-1 and syntaxin 8 (20) or GLUT4 and VAPA (15) indicated that components of the vSNARE or tSNARE complex might have functions besides regulating exocytosis, as they modulate channels or transporters which are integral to the surface/cell membrane.

MATERIALS and METHODS

Split-ubiquitin Yeast Two-Hybrid experiments

A split-ubiquitin Yeast Two-Hybrid membrane protein system (Y2H Membrane Protein Kit, MoBiTec, Göttingen, Germany) was used for screening a NubG fused human brain cDNA library in the yeast strain NMY51 to identify potential interaction partners of HCN2. For this purpose full-length mHCN2 was subcloned by *Sfi*I restriction sites into the bait vector pBT3-N according to the instruction manual (MoBiTec, Göttingen, Germany). pAl-Alg5 was used as positive control and pPR3-N as negative control. Yeast clones were selected by activation of reporter genes upon positive interaction of bait (pBT3-mHCN2) and prey (NubG-x fused cDNA library) encoding two auxotrophic growth markers (HIS3 and ADE2). Activation of reporter genes concedes yeast clones to grow on minimal medium lacking histidine (H), adenine (A), leucine (L) and tryptophan (W) for selection (-LWHA medium). Further selection for the strongest interactors was performed by a β-galactosidase assay due to the property of positive colonies expressing the protein β-galactosidase. Isolated plasmid-DNA of positive yeast colonies was analyzed by sequencing. For the confirmation of interaction, a split ubiquitin Yeast-Two-Hybrid direct interaction assay was performed. Therefore, full-length hVAPB was subcloned via *Sfi*I restriction sites into the prey vector pPR3-N and tested for an interaction with pBT3-mHCN2 or pBT3-hHCN4 by validation of colony growth on minimal medium (-LWHA).

Expression constructs

For oocyte expression hHCN1, mHCN2, hHCN4 and hVAPB were subcloned into pSGEM. ^{NTK}HCN2 was cloned into ALMV vector and mHCN2$^{HA_{Ex}}$ into pBF1. cRNA was prepared with mMessage mMachine T7 or SP6 Kit (Ambion, Thermo Fisher Scientific, Waltham, MA) after linearization. QuikChange (Stratagene, Biocompare, South San Francisco, CA) mutagenesis kit was used to introduce specific mutations. hVAPB, hVAPA, hVAMP1 and hVAMP2 were subcloned in frame into the pGEX-4T-1 vector (Amersham, GE Healthcare, Freiburg, Germany) for GST-fusion protein expression in BL21 cells. VAPB and VAPA were subcloned via EcoRI and SalI, whereas VAMP1 and VAMP2 were subcloned with BamHI and EcoRI. Constructs for mammalian cell expression were subcloned in pEGFP, pDsRed or pcDNA3.1(+) vectors.

GST pull-down experiments

GST-fusion proteins were obtained after lysis of 1 ml BL21 cell culture. Protein expression was induced at 0.4-0.6 OD_{600} by 1 mM IPTG for 3 h at 37 °C. Protein extraction of a 1 ml culture was performed using 200 µl RIPA buffer supplemented with 4 µl protease inhibitor cocktail (PIC) (Sigma-Aldrich, Merck, München, Germany) and 1% lysozyme. Six freeze and thaw cycles were performed to improve the protein yield. HCN2 protein was prepared by lysis of HeLa cells transfected with 2 µg $HCN2^{EGFP}$. HeLa cells were harvested 48 h after transfection, washed in PBS and lysed 30 min on ice using 200 µl RIPA buffer supplemented with 10 µl PIC (Sigma-Aldrich, Merck, München, Germany). Insoluble material was separated by centrifugation (13.000 rpm for 15 min at 4 °C). TnT® Quick Coupled Transcription/Translation System (T7, Promega, Madison, WI) was used to synthesize *in vitro* translated HCN2 based on HCN2 pcDNA3.1 plasmid using T7 promotor. Pull-down experiments were performed following the MagneGST Pull-Down System (Promega, Madison, WI) manual. Proteins were eluted from magnetic beads with 20 µl 2x SDS sample buffer. For separation of the proteins by SDS-PAGE, pull-downs were heat denatured at 40 °C for 10 min. After centrifugation at 5.000 rpm for 3 min protein lysates were separated on a 8% SDS-polyacrylamide gel. The input illustrated in **Fig. 1*C-D*** was diluted 1:15 and 1:10 in **Fig. 1*F***. Proteins were transferred to a nitrocellulose membrane via a Semi-Dry Transfer Cell (Biorad, Müchen, Germany) at 70 mA for 1 h. For GST pull-downs with $HCN2^{EGFP}$, the HCN2 protein was visualized by immunoblotting with mouse α-GFP antibody (#ab290, 1:5000, abcam, Cambridge, United Kingdom). The binding of the primary antibody was detected using peroxidase-conjugated goat α-rabbit IgG antibody (#32460, 1:2000, Pierce Thermo Scientific, Waltham, MA) and a chemiluminescent extended-duration substrate (Super Signal West Dura, Thermo Scientific, Waltham, MA). Untagged HCN2 protein was detected with rabbit α-HCN2 antibody (#APC-030, 1:300, Alomone, Jerusalem, Israel) and peroxidase-conjugated goat α-rabbit IgG antibody (#32460, 1:2000, Pierce Thermo Scientific, Waltham, MA) as the secondary antibody.

Two-electrode voltage-clamp (TEVC) measurements in Xenopus oocytes

Isolation of *Xenopus laevis* oocytes and TEVC recordings were performed as previously described (21). Stage IV and V oocytes were injected with 7.5 ng of HCN2 cRNA or co-injected with 1 ng of VAPB, $VAPB^{P56S}$, VAPA, VAPC, VAMP1 and VAMP2, as well as 1 ng

of the following VAPB mutations: TM^{VAPB}, MSP^{VAPB}, $MSP\text{-}CC_{0.5}{}^{VAPB}$ and $MSP\text{-}CC^{VAPB}$. For the C-terminal deletion constructs 3.5 ng $^{NTK}HCN2$, $HCN2^{F530*}$ and $HCN2^{V628*}$ or 15 ng of $HCN2^{F486*}$were co-expressed with 1 ng VAPB. To determine selectivity within HCN-channel family members 3.5 ng HCN1 or 15 ng HCN4 cRNA was co-expressed with 1 ng VAPB. 3.5 ng HCN2 was co-expressed with 0.25 ng VAPA/B complex. TEVC experiments were performed in ND96 solution, containing (in mM): NaCl 96, KCl 2, $CaCl_2$ 1.8, $MgCl_2$ 1, HEPES 5; pH 7.4, 2 days after injection of the respective constructs. ND66 solution, containing (in mM): NaCl 66, KCl 32, $CaCl_2$ 1.8, $MgCl_2$ 1, HEPES 5; pH 7.4, was used for the co-expression experiments of VAPB with HCN4, $HCN2^{F486*}$ and the complex measurements of HCN2 and VAPA/B, due to small current amplitudes. IV-curves were recorded by two second voltage steps to potentials ranging from -30 mV to -140 mV from a holding potential of -30 mV. Tail currents were recorded by a 750 ms test pulse to -130 mV.

Inside-out macropatch clamp recordings from Xenopus laevis oocytes

Giant patch recordings in the inside-out configuration under voltage-clamp conditions were made at room temperature (22 - 24 °C). Pipettes were made from thick-walled borosilicate glass, had resistances of 0.3 - 0.5 MΩ (tip diameter of 5 - 15 µm) and were filled with a pipette solution containing (in mM): KCl 120, HEPES 10 and $CaCl_2$ 1.0; pH 7.2. Bath solutions had the following composition (in mM): KCl 100, HEPES 10, K_2EGTA 10; pH 7.2. Bath solutions were applied via a multi-barrel pipette system to the cytoplasmic side of excised membrane patches. Currents were recorded with an EPC10 amplifier (HEKA electronics, Lambrecht, Germany) and capacitive transients were compensated with an automated circuit of the EPC10.

Fluorescence microscopy

HeLa or HL-1 cells were grown on 35 mm glass bottom Petri dishes (Willco, Amsterdam, Netherlands) to a confluency of about 50%. HeLa cells were grown in DMEM medium containing 10% fetal bovine serum (Invitrogen, Thermo Scientific, Waltham, MA) and 1% Pen Strep (Life Technologies, Darmstadt, Germany). After 24 h, HeLa cells were transfected with either 1 µg EGFP-C1-HCN2-HA_{Ex} ($^{EGFP}HCN2^{HA_{Ex}}$) or co-transfected with VAPB pcDNA3.1 or TM^{VAPB} pcDNA3.1 per dish using Jetprime (Peqlab, Erlangen, Germany). Cells were maintained at 37 °C for 6 - 48 h aerated with 5% CO_2. For fluorescence imaging HL-1

cells were fixed with methanol, while for HeLa cells live cell imaging in a HBSS buffer (Invitrogen, Thermo Scientific, Waltham, MA) was performed. Fixed HL-1 cells were stained with an α-VAPB antibody (#sc-98992, 1:50, Santa Cruz, Heidelberg, Germany) after permeabilization (0.25% Triton-X-100/PBS) and blocking with 3% goat serum/PBS. For visualization an Alexa Fluor 488 goat α-rabbit antibody (#A11008,1:200, Invitrogen, Thermo Scientific, Waltham, MA) was used. Fluorescence microscopy was performed with an Olympus IX71 microscope equipped with a 60× N.A. 1.3 PL APO objective or a 100× N.A. 1.4 PL APO objective (Olympus, Hamburg, Germany), standard EGFP/Texas Red filter sets and a cooled 12-bit CCD camera (SensiCam QE). During live cell imaging, cells were maintained at 37 °C using an objective heater (Bioptechs, Butler, PA). Digital images were processed using Image-Pro Plus 6.0 (MediaCybernetics, Cambridge, United Kingdom).

Analyses of channel surface expression in oocytes and HeLa cells and Western blot analysis

Xenopus laevis oocytes were injected with 10 ng $HCN2^{HA_{Ex}}$ cRNA transcribed from pBF1 alone or co-expressed with 1 ng VAPB 48 h before surface expression analysis. Subsequently, a chemiluminescence assay was performed as previously described (21).

For surface expression studies in HeLa cells, cells were grown to a confluency of 90% and transfected with either 1 µg $^{EGFP}HCN2^{HA_{Ex}}$ alone or co-transfected with 1 µg VAPB pcDNA3.1 or TM^{VAPB} pcDNA3.1. Cells were fixed with 4% PFA for 20 min on ice and blocked with 10% normal goat serum/PBS with 0.1% sodium azide for 1 h at room temperature. Immunolabeling was performed with an α-HA antibody (#sc-7392, 1:100 in PBS, Santa Cruz, Heidelberg, Germany) for 1 h followed by 4 times washing in PBS. After incubation with a peroxidase-coupled secondary antibody (#sc-2005, α-goat, 1:5000, Santa Cruz, Heidelberg, Germany) luminescence was measured in a luminometer (GloMax® 20/20, Promega, Madison, WI) by addition of chemiluminescence substrate (SuperSignal ELISA Femto Maximum Sensitivity Substrate, Thermo Scientific, Waltham, MA). Peak luminescence was determined and normalized to $^{EGFP}HCN2^{HA_{Ex}}$ mean luminescence. For determination of the whole cell protein concentration, cells were lysed with RIPA buffer as previously described. Equal amounts of protein lysates verified by Bradford assay were separated on a 10% SDS-polyacrylamide gel with Mini-PROTEAN Tetra Cell (Biorad, Müchen, Germany) at 35 mA and transferred to a nitrocellulose membrane for Western blot

analysis. $^{EGFP}HCN2^{HA_{Ex}}$ was detected with an α-GFP antibody (#ab290, 1:5000, abcam, Cambridge, United Kingdom).

Preparation and transfection of primary cortical neurons

Primary cultures of cortical neurons were prepared from embryonic Sprague-Dawley rats (E16) (*Rattus norvegicus*) essentially as previously described (22). Primary cortical neurons were seeded at a density of 200.000 cells/well (24 well plates) onto polylysine-coated coverslips in Neurobasal A medium supplemented with 2% B27, 1 µg/µl gentamycin, 2 mM glutamax, and 5% FCS. After 4 h, this medium was replaced with Neurobasal medium supplemented with 1.2 mM glutamine, 2% (v/v) B27 supplement (20 ml/l) and penicillin/streptomycin (0.1 mg/ml) which was used as a culture medium. Following 3-DIV, neurons were transfected with 1 µg HA-tagged VAPB (^{HA}VAPB) or $^{HA}VAPB^{P56S}$ plasmid using 2 µl/ml Lipofectamine2000 (Invitrogen, Thermo Scientific, Waltham, MA) according to the manufacturer's instructions.
Images were acquired using a confocal laser scanning microscope (Leica SP5, Wetzlar, Germany). Light was collected through a 63x 1.4 NA oil immersion lens with an additional 2× optical zoom applied for dendritic regions. For green detection, cells were excited at 488 nm and 543 nm and emissions were detected using 505-530 band pass filter (green), Alexa 568 stained HCN2 or VAPB was detected by excitation at 620 nm band pass filter and emission by using a 690 nm long pass filter (red).

In-situ hybridization

To generate specific ISH probes cDNA fragments of HCN2 (nt. 1404-1934, NM_008226.2), VAPA (nt. 894-1462, NM_013933.3) and VAPB (nt. 3299- 4320, NM_019806.5) were obtained by RT-PCR cloning from RNA extracts of mouse brain and subcloned into pGEM-T (Promega, Madison, WI) for *in vitro* transcription. Specific primer sets are listed in Supplemental Table 1. 14 µm thick frozen brain sections were cut on a LEICA cryostat, thaw-mounted on adhesive slides and subjected to the pre-hybridization procedure as described. Digoxigenin (Dig)-labeled probes in anti-sense and sense orientation were generated from the templates described above by *in vitro* transcription using SP6 or T7 RNA polymerase in a Dig labeling mix containing 10 mM each of ATP, CTP, and GTP, 6.5 mM UTP and 3.5 mM

digoxigenin-11-UTP (Roche, Mannheim, Germany). Riboprobes in sense-orientation served as negative controls. After limited alkaline hydrolysis (0.2 M Na_2CO_3, pH 10.2) probes were added to the hybridization solution (3× SSC, 50 mM Na_3PO_4, 10 mM dithiothreitol, 1× Denhardt's solution, 0.25 g/l yeast tRNA, 10% dextran sulfate, and 50% formamide) to a final concentration of 0.1 to 0.5 ng/µl. To each slide 50 µl hybridization mix was applied and incubated for 14 h at 60 °C. Slides were washed in 2× SSC for 20 min, followed by 30 min RNase A treatment [20 µg RNase A and 1U/ml RNase T1 (Roche, Mannheim, Germany) in 10 mM Tris-HCl, pH 8.0, 0.5 M NaCl, and 1 mM EDTA] at 37 °C. The slides were washed at room temperature in decreasing salt concentrations (1, 0.5, and 0.2× SSC) for 20 min each and at 60 °C in 0.2× SSC for 1 h, followed by a final rinse at room temperature in 0.2× SSC and distilled water for 10 min each. For hybrid detection slides were equilibrated for 30 min at room temperature in buffer A (100 mM Tris and 150 mM NaCl, pH 7.5) containing 0.05% Tween 20 (Merck, Darmstadt, Germany) and blocking reagent (Roche, Mannheim, Germany). Alkaline phosphatase-conjugated anti-Dig Fab fragments (#11093274910, Roche, Mannheim, Germany) were diluted to 0.25 U/ml in blocking buffer and applied to slides for 2 h at 37 °C. Excessive antibody was removed by two 10 min washes in buffer A. Slides were equilibrated to buffer B (100 mM Tris, 100 mM NaCl, and 50 mM $MgCl_2$; pH 9.4) containing 0.05% Tween 20 for 10 min. The chromogen solution containing 0.2 mM 5-bromo-4-chloro-3-indolyl phosphate and 0.2 mM nitroblue tetrazolium salt (Roche, Mannheim, Germany) in buffer B was applied for 3 to 12 h in the dark, under periodic microscopic monitoring of color development, until reaction was stopped in water. Slides were embedded in aqueous mounting medium (Merck, Darmstadt, Germany). Only adult (3 - 6 months) in house bred male C57BL6/J mice were used (n = 4). Each ISH experiment was performed three times and for each brain region investigated nine to twelve sections (equals three to four slides) were hybridized with anti-sense probes and six sections (two slides) with sense probes. For analysis and documentation an Olympus AX70 fluorescence microscope (Olympus Optical, Hamburg, Germany) equipped with a SPOT digital camera system (Diagnostics Instruments Inc, Sterling Heights, MI) was used.

VAPA and VAPB knock-down experiments in embryonic zebrafish

Zebrafish (*Danio rerio*) of the Tübingen strain were bred and maintained at 28.5 °C as described by Westerfield (23). Pictures and movies were recorded at 72 hours post fertilization (hpf). Heart rate was counted at 72 hpf at room temperature. For all Morpholino-

modified antisense oligonucleotide injection procedures, the TE wild-type strain was used. Morpholino-modified antisense oligonucleotides (MO) (Gene Tools, LLC, Philomath, OR) were directed against the translational start site (5'-TCAGGATCTGCTCCAGTTTGGACAT-3') of zebrafish VAPA (^{MO}VAPA), and the translational start site (5'-CCATCTCCCACTGC-AAACGCTCGGA-3') of zebrafish VAPB (^{MO}VAPB). For rescue experiments, sense-capped cRNAs of human wild-type VAPA as well as wild-type and mutant VAPB^{P56S} were synthesized using the mMESSAGE mMACHINE system (Ambion, Thermo Fisher Scientific, Waltham, MA). Each cRNA was, with a concentration of 75 ng/µl, co-injected with ^{MO}VAPB or KCl. Calcium imaging was performed as previously described (24, 25). Wild-type and ^{MO}VAPA/VAPB morphant embryos were injected with 1 nl of a 250 µM stock solution of calcium green-1 dextran (Molecular Probes) at the one-cell stage. At 72 hpf videos were recorded with a Proxitronic (Proxivision, Bensheim, Germany) camera at 29.97 frames per second. Relative fluorescence of the atrium and ventricle were analyzed with custom-made software (26). All zebrafish injection procedures were repeated at least three times (three biological replicates). All surviving injected embryos per group were subjected to functional analyses at 72 hpf.

Immunostaining of VAPB in embryonic zebrafish hearts

Dissected hearts of 72 hpf old zebrafish embryos were fixed in 4% methanol-free formaldehyde in PBS. After blocking in 10% goat-serum in PBST, hearts were incubated with a custom made rabbit polyclonal anti-mouse VAPB antibody (1:2000), previously described (37), for 1 h at RT. The secondary antibodies were diluted 1:1000 in PBST and incubated for 30 min at RT. For documentation a Zeiss Axioskop2 plus and the Axio Vision software (Zeiss, Wetzlar, Germany) was used.

RT-PCR and in-situ hybridization

RNAs from embryonic zebrafish hearts were extracted using the RNeasy® Mini Kit (Qiagen, Hilden, Germany) according to the manufacturer's instructions. Reverse transcription was performed by using SuperScript® III Reverse Transcriptase (Life Technologies, Darmstadt, Germany). *Vapa*- and *vapb*-specific PCR analyses were carried out according to standard protocols using SYBR-Green master mix (Roche, Germany) and a Roche LightCycler 480 II. Whole-mount *in-situ* hybridization was performed using Digoxigenin-labelled antisense RNA probes against zebrafish vapa and vapb as previously described.

ECGs in VAPB$^{-/-}$ mice

Non-invasive surface ECGs from adult VAPB (+/+, +/-, -/-) mice (C57Bl/6N tac strain) gently restrained by an ECG tunnel system (EMKA Technologies, Paris, France) were recorded by contact electrodes inserted in the tunnel floor in conscious mice. VAPB knock-out mice were backcrossed over five generations and for the experiments wild-type littermates served as control. All parameters were measured from lead I by blinded observers.

Experiments in HL-1 cells

HL-1 cells were grown on 35 mm dishes (Nunc, Thermo Fisher Scientific, Waltham, MA) to a confluency of about 50%. Cells in each dish were either transfected with 2 µg pEGFP vector alone, or in combination with 2 µg VAPB pcDNA3.1(+) or 2 µg pcDNA3.1(+). For knock-down experiments HL-1 cells were transfected with either 2 µg shVAPB-GIPZ or 2 µg shcontrol-GIPZ. For Western blot analysis of HL-1 cardiomyocytes, the cells were treated with puromycin to select for transfected cells. After 24 hours, HL-1 cells were measured with an EPC10 amplifier (HEKA electronics, Lambrecht, Germany) in the whole-cell configuration at room temperature (22 °C) using previously described solutions (27). Pipettes had a tip resistance of 2.5 - 4.0 MΩ when filled with a solution for I_f recordings containing (in mM): KCl 120, TEA-Cl 10, Na_2GTP 0.4, Na_2ATP 5, $MgCl_2$ 2, EGTA acid 11, $CaCl_2$ 5 and HEPES 5; pH 7.2. Cells were bathed in modified Tyrode solution containing (in mM): NaCl 140, KCl 25, $MgCl_2$ 1.2, $CaCl_2$ 1.8, glucose 10, $NiCl_2$ 2, $BaCl_2$ 2, 4-aminopyridine 0.5 and HEPES 5; pH 7.4. Series resistances were automatically compensated by 70%. IV-relationships were recorded by 1.5 s voltage steps ranging from -20 mV to -120 mV in 20 mV increments, recorded from a holding potential of -30 mV with a sweep time interval of 10 s. Tail currents were elicited by a 300 ms step to -110 mV.

For action potential measurements HL-1 cells were grown to 100% confluency and action potentials were measured in the current clamp mode without electrical stimulation. Pipettes had a resistance between 2.5 - 4.0 MΩ, when filled with a solution containing (in mM): KCl 60, K-glutamate 65, Na_2GTP 0.2, K_2ATP 3, $MgCl_2$ 2, EGTA 5, and HEPES 5; pH 7.2. Whole-cell measurements were obtained at room temperature in a bath solution containing (in mM): NaCl 135, KCl 5, $MgCl_2$ 1, NaH_2PO_4 0.33, glucose 10, Na-pyruvate 2, $CaCl_2$ 1 and HEPES 10; pH 7.4.

Slice patch clamp experiments of neurons of the piriform cortex and the thalamus

Animals were sacrificed under isoflurane anesthesia and brain tissue was rapidly removed from the skull. Thalamic coronal slices (250 µm) were prepared from $VAPB^{-/-}$ and C57Bl/6N tac mice (p90-p120) on ice-cold oxygenated (O_2) saline solution, containing (in mM): sucrose 200, PIPES 20, KCl 2.5, NaH_2PO_4 1.25, $MgSO_4$ 10, $CaCl_2$ 0.5, dextrose 10; pH 7.35. Slices were transferred to a chamber with an artificial cerebrospinal fluid (ACSF) containing (in mM): NaCl 125, KCl 2.5, NaH_2PO_4 1.25, $NaHCO_3$ 24, $MgSO_4$ 2, $CaCl_2$ 2, dextrose 10; and kept for 30 min at the temperature of 30-32 ºC and further at room temperature until the recording time. pH was adjusted to 7.35 by constant aerating with carbogen (95% O_2 and 5% CO_2). I_h was recorded in the whole-cell mode from thalamocortical neurons (TC) of the ventrobasal thalamic complex (VB) and pyramidal neurons of piriform cortex (Pir). Slices were transferred to a recording chamber with an external solution (bath solution) containing (in mM): NaCl 120, KCl 2.5, NaH_2PO_4 1.25, HEPES 30, $MgSO_4$ 2, $CaCl_2$ 2, dextrose 10; pH 7.25. Recordings were performed at 30 ± 1 ºC. Patch pipettes were pulled from borosilicate glass (GC150T-10; Clark Electromedical Instruments, Kent, United Kingdom) and had resistances of 3 - 5 MΩ. The pipette solution contained (in mM): K-gluconate 95, K_3-citrate 20, NaCl 10, HEPES 10, $MgCl_2$ 1, $CaCl_2$ 0.5, BAPTA 3, MgATP 3, Na_2GTP 0.5; pH 7.25 and 295 mOsm/kg. All recordings were made from the soma of the neurons using an EPC10 amplifier (HEKA electronics, Lambrecht, Germany). The access resistance was in a range of 5 - 25 MΩ and was monitored throughout the whole experiment. Cells with access resistance more than 25 MΩ were discarded. Series resistance compensation of >30% was applied. Voltage-clamp experiments were controlled by the software Pulse or PatchMaster (HEKA electronics, Lambrecht, Germany). Measurements were corrected for a liquid junction potential of 10 mV. The protocol used for assessment of I_h current is as described previously (5). Briefly, I_h current was measured by hyperpolarizing steps of -10 mV increment from a holding potential of -40 to -130 mV.

Immunohistochemistry of HCN channels in the piriform cortex

Twenty to thirty day-old mice C57BL/6NTac were transcardially perfused with 4% PFA. Brains were removed and post fixed for 2 hours in 4% PFA and later in 30% sucrose for 48 hours. Free-floating coronal sections (40 µm) were cut and slices were collected in phosphate-

buffered saline (PBS). Sections were washed 3 times for 10 min in PBS, preincubated for 20 minutes in PBS containing 0.3% Triton-X100. Slices were then incubated for 2 hours in 6% normal goat serum in PBS/Triton-X100 0.3%. Slices were incubated with primary antibodies: rabbit(rb)-anti-HCN1 (#APC-056, 1:200), rb-anti-HCN2 (#APC-030, 1:200), rb-anti-HCN4 (#APC-052, 1:200) (Polyclonal rabbit-antibodies, Alomone labs, Israel) and guinea pig (gp)-anti-Map2 (#188004, 1:100, Synaptic Systems, Germany) for 48 hours at 4 °C. After incubation with the primary antibody, slices were washed 3 times for 10 minutes in PBS and thereafter transferred to the secondary antibody solution (Alexa Fluor 568 goat anti-gp-IgG, #ab175714, 1:1000 and Alexa Fluor 488 goat anti-rb-IgG, #ab150113, 1:1000) for one hour, washed 3 times thereafter for 10 min and mounted with a mounting medium (VECTASHIELD with DAPI, Vector Laboratories Inc., Burlingame, CA, USA) for confocal microscopy.

Patch clamp recordings of I_{Na} and I_{Ca} in iPSC-derived cardiomyocytes

Whole-cell patch clamp experiments for measurement of Ca^{2+} and Na^{+} currents were performed in murine iPSC-derived cardiomyocytes (iPSC-CMs, commercially available from Axiogenesis AG, Cologne, Germany, http://axiogenesis.com/). Cells were seeded in 35 mm glass bottom dishes (MatTek, Ashland, MA) coated with laminin and fibronectin at a density of $2x10^4$ cells per dish. Cells were incubated at 5% CO_2 and 37 °C with CorAt media. Cells were transfected with pEGFP empty vector (200 ng) either with pcDNA3.1(+) vector (1 µg) as control or with VAPB pcDNA3.1(+) (1 µg) using Lipofectamin 3000 (Invitrogen, Thermo Scientific, Waltham, MA) following manual instructions. Currents were measured 48-72 hours after transfection with glass electrodes (1.5-5 MΩ) filled with intracellular solution containing (in mM): NaCl 8, CsAsp 120, TEA-Cl 20, $MgCl_2$ 5.9, HEPES 20 and K_2ATP 5, pH 7.2. An EPC-10 amplifier (Heka electronics, Lambrecht, Germany) and the Fitmaster program (Heka electronics, Lambrecht, Germany) was used for data acquisition. For measurements of the Ca^{2+} currents (I_{Ca}), cells were kept in normal tyrode solution (in mM: NaCl 140, KCl 5.4, $MgCl_2$ 1.1, HEPES 5, glucose 10, $CaCl_2$ 1.8, pH 7.4) supplemented with CsCl (5 mM). Whole-cell currents were recorded from a holding potential of −80 mV, using a 500 ms voltage-ramp from -80 mV to -40 mV to inactivate sodium currents before *I-V* measurements. Starting from a test potential of -40 mV, cells were clamped to different voltages in 400 ms steps ranging from -50 mV to +40 mV in 10 mV increments. Sodium currents (I_{Na}) were elicited in a bath solution containing (in mM): NaCl 20, NMDG 120, KCl

4, $MgCl_2$ 1, $CaCl_2$ 1.8, HEPES 5, glucose 10, pH 7.4, supplemented with 5 µM nifedipine. Whole-cell currents were recorded from a holding potential of −80 mV followed by 100 ms voltage steps from -80 mV to +40 mV in 5 mV increments.

Patch clamp recordings of Cav1.3 in HEK293 cells

HEK293 cells were cultured in 25 cm^2 flasks at 37 °C and 5% CO_2 in DMEM (Invitrogen, Thermo Scientific, Waltham, MA) supplemented with 10% FCS and 1% penicillin/streptomycin solution (Invitrogen, Thermo Scientific, Waltham, MA). At a confluency of 60 - 70%, cells were transiently transfected with complementary DNA encoding Cav1.3 α_1-subunits (human, 6 µg/flask) together with auxiliary β_{2b} (human, 3 µg/flask) and $\alpha_2\delta_1$-subunits (human, 3 µg/flask), EGFP (0.5 µg/flask) and empty vector (pcDNA3.1(+), 3 µg/flask) or VAPB (human, 3 µg/flask) using JetPRIME (Peqlab, Erlangen, Germany). Cells were subsequently kept at 30 °C and 5% CO_2. 48 h after transfection cells were detached using 0.05% trypsin and transferred to 35-mm Petri dishes for electrophysiological recordings. Whole-cell patch-clamp recordings were performed at room temperature with an EPC10 amplifier (HEKA electronics, Lambrecht, Germany) using electrodes pulled from borosilicate capillaries with a resistance of 2 - 5 MΩ. Series resistance was compensated by 50%. The extracellular solution contained 110 mM NaCl, 20 mM CsCl, 10 mM $BaCl_2$, 10 mM HEPES, 1 mM $MgCl_2$ and 10 mM glucose (pH 7.4). The pipette internal solution contained 130 mM KCl, 10 mM NaCl, 0.5 mM $MgCl_2$, 1 mM EGTA and 5 mM HEPES (pH 7.3). Current–voltage (*I–V*) relationships were obtained by applying a 300 ms long square pulse protocol to various test potentials starting from a holding potential of -80 mV.

Cell culture

HEK293 and HeLa cells were obtained from Sigma-Aldrich® and mouse iPSC-CMs from Axiogenesis® which were not authenticated again after commercial purchase. HL-1 cells were previously obtained by Prof. Claycomb and authenticated by their electrophysiological properties (21). All cells were probed for mycoplasma contamination.

Quantification and statistical analysis

Statistics were performed as previously described (28). Briefly, every dataset for wild-type and each mutant and for every current/kinetical feature analyzed was tested with a Shapiro-Wilk test for normality. Equality of variances was tested using either a parametric or non-parametric Levene's test. In case of similar variances, significance was probed using either a paired or unpaired Student´s t-test and for not normally distributed data, a non-parametric Mann-Whitney U-test and a Wilcoxon signed-rank test for paired analyses was used, respectively. If the variances of the groups were different, significance was probed using either Welch's t-test and for not normally distributed data Mood's median test was used. Experiments were non-randomized and non-blinded and no pre-specified sample size was estimated. For inclusion/exclusion criteria, only dead embryonic zebrafish were excluded from the statistics. For experiments using $VAPB^{-/-}$ mice, we have based estimated differences on previous data and calculations of sample size assuming $1 - \beta = 0.80$ and $\alpha = 0.05$. To detect changes in ECG recordings, at least eight animals per genotype were used, to ensure adequate power to detect 20-30% change. All alive and healthy looking littermate animals were examined. ECG recordings of all examined mice was high enough in quality for analyzing heart rate, PQ interval, QT interval and duration of QRS complex following pre-established criteria. T-wave morphology analysis of three mice had to be excluded because signals were divergent from pre-established criteria. The order of taking ECGs recordings was randomized to consecutive order following cage numbers which were marked by the animal facility. The investigators performing and analyzing the ECGs were blinded to the genotype.

Ethical Approval

The investigation conforms to the Guide for the Care and Use of Laboratory Animals (NIH Publication 85-23). All experimental procedures were performed in accordance with the principles approved by local authorities (review board institution: Landesamt für Natur, Umwelt und Verbraucherschutz Nordrhein-Westfalen, Germany; approval IDs: 84-02.04.2015.A574, 84-02.05.50.15.026 and 887-50 10 37 09.125) or the UK Home Office (PPL number 30/2967). Efforts were made to minimize the number of animals and the degree of discomfort to animals used in this study.

RESULTS

VAPB selectively increases HCN1 and HCN2 pacemaker currents

Using a split-ubiquitin Yeast Two-Hybrid (Y2H) (29) screen with the full-length HCN2 channel as a bait to search for plasma membrane bound channel modulators, we identified from a human adult brain cDNA library VAPB as a potential HCN2 interacting partner. From 458 clones that grew under drop out conditions 35 clones contained VAPB. In contrast, VAPA, the closest relative of VAPB, was not fished from the human brain cDNA library. Y2H direct-interaction assays confirmed an interaction of VAPB with HCN2, but not HCN4 **(Fig. 1*A*)**. VAP proteins are anchored with a C-terminal transmembrane domain (TM) in the cell membrane, contain a conserved N-terminal major sperm region (MSP) and an amphipathic coiled-coil domain (CC), which is a common motif in tSNAREs (30) **(Fig. 1*B*)**. The VAPB fragments identified through the Y2H screen include the TM and parts of the CC, but not the MSP domain (Supplemental Fig. 1). GST pull-down experiments confirmed an interaction of HCN2 with VAPB **(Fig. 1*C*)**, but also the close family member VAPA and the VAP-interacting partners VAMP1 and VAMP2 **(Fig. 1*D*)**. Using HCN2 transfected HeLa cells ^{GST}VAPA pulled down HCN2 together with endogenously expressed VAPB, suggesting that HCN2 channels might be in a complex with VAPA and VAPB **(Fig. 1*E*)**. VAPB and VAPA both directly interact with *in vitro* translated HCN2, albeit the physical interaction with VAPA seems to be more efficient **(Fig. 1*F*)**. Pull-down experiments with *in vitro* translated HCN2 confirmed also a direct interaction with VAMPs **(Fig. 1*F*)**. Most importantly, both ^{GST}VAPA and ^{GST}VAPB pulled down HCN2 from rat brain protein lysates **(Fig. 1*G*)**.

The co-expression of HCN2 with low amounts of VAPB in *Xenopus* oocytes strongly increased current amplitudes **(Fig. 1*H, I*)**. HCN1 current amplitudes were also increased **(Fig. 1*J*)**, while HCN4 was not modulated, consistent with our interaction analyses **(Fig. 1*A, J*)**. None of the other tested potassium channels were influenced by VAPB, revealing a selectivity for HCN1 and HCN2 channels **(Fig. 1*K*)**. To further support this observation, we performed patch clamp experiments of mouse iPSC cardiomyocytes (iPSC-CMs) transfected with VAPB, to probe for effects of VAPB on cardiac sodium and calcium channels. Here VAPB transfection did not alter inward sodium (I_{Na}) or calcium (I_{Ca}) currents (Supplemental Fig. 2*A-F* and Material and Methods). In addition, as these iPSC-CMs rather reflect ventricular cardiomyocytes than sino-atrial pacemaker cells, we also excluded that VAPB modulates

Cav1.3, a channel highly relevant for sino-atrial pacemaking (Supplemental Fig. 2*G-I*). The VAP family contains an alternative spliced isoform, VAPC, lacking the CC and the TM domains (17, 31). Whereas VAPA also mildly increases the HCN2 current amplitudes, VAPC has no modulatory effect (**Fig. 1*L*** and Supplemental Fig. 3). Strikingly, co-expressing HCN2 together with VAPA and VAPB led to a similar and slightly more pronounced current increase **(Fig. 1*M*)**, compared to VAPB co-expressed alone **(Fig. 1*L*)**. Albeit the current increase was not significantly larger, the effect was more robust (compare HCN2 + VAPB, $p<0.01$ versus HCN2 + VAPA/VAPB, $p<0.001$) (**Fig. 1*L, M***).

VAPB did not alter the voltage-dependence of HCN2 activation (Supplemental Fig. 4*A*) or the activation kinetics (Supplemental Fig. 4*B*), a similar lack of effects was observed for VAPA and VAPC (Supplemental Fig. 3). As effects of VAPB on the voltage-dependence of activation might be missed due to the high cAMP-levels intrinsic to oocytes, we performed inside-out macropatch clamp recordings from oocytes to directly control intracellular cAMP concentrations. However, also in inside-out patches and in absence of intracellular cAMP, VAPB did not influence the voltage-dependence of activation **(Fig. 1*N-Q*)**. In addition, application of 100 µM cAMP maximally shifted the voltage-dependence of activation in a similar manner, as for HCN2 alone, indicating that there is no effect of VAPB on the cAMP-modulation of the channels **(Fig. 1*N-Q*)**.

Next, we investigated the mechanism for the increased HCN2 current amplitudes. The current amplitudes of HCN2, now harboring an extracellular HA-epitope ($HCN2^{HA_{Ex}}$) was increased, similar as described for the untagged protein **(Fig. 1*R*)**. The surface expression in the same oocytes, probed with a chemiluminescence-assay (ELISA), exclusively detecting channels at the plasma membrane, revealed that the increased current amplitudes are mainly caused by an increased surface expression of the channels **(Fig. 1*R, S*)**.

The previously described $VAPB^{P56S}$ mutation located in the MSP domain causes ALS8 and late onset spinal muscular atrophy (32). Co-expression of $VAPB^{P56S}$ with HCN2 revealed that the ALS-causing mutation lost its ability to increase the HCN2 current amplitudes **(Fig. 1*T*)**.

Domains mediating the interaction of VAPB with HCN2

A split-ubiquitin Y2H direct-interaction assay introducing different premature stop codons in HCN2 revealed that the CNBD and the entire C-terminus are dispensable for the interaction with VAPB and that the N-terminus of HCN2 together with the S1 segment is sufficient for the interaction (**Fig. 2*A, B*** and Supplemental Fig. *5*). These data are supported by functional

studies **(Fig. 2*C*)** in which VAPB still increased the current amplitudes of HCN2 channels which lack the entire C-terminus ($HCN2^{F486*}$) **(Fig. 2*C*)**. In contrast, current amplitudes of HCN2 channels with an N-terminal deletion ($^{NTK}HCN2$) (33) were no longer modulated by VAPB **(Fig. 2*D*)**. Consistently, the $^{NTK}HCN2^{HA_{Ex}}$ current amplitude **(Fig. 2*E*)** and surface expression **(Fig. 2*F*)** were not altered by VAPB. Similar effects were obtained replacing the N-terminus of HCN2 by that of HCN4 ($^{HCN4\text{-}N}HCN2$) which also results in a loss of VAPB modulation **(Fig. 2*G*)**.

Next, we probed which parts of VAPB mediate the functional effects on HCN2. Surprisingly, the transmembrane segment of VAPB alone (TM^{VAPB}) is sufficient to increase HCN2 currents **(Fig. 2*H*)**, while the MSP domain alone or in combination with the CC domain ($MSP+CC^{VAPB}$) is ineffective. These data are consistent with the lack of HCN2 modulation by VAPC which lacks the TM domain (17). Confirming the role of the transmembrane segment for channel modulation, also the $HCN2^{HA_{Ex}}$ current amplitudes **(Fig. 2*I*)** and surface expression **(Fig. 2*J*)** were increased by TM^{VAPB}.

VAPB determines surface expression and dendritic localization of HCN2

Co-transfection of N-terminally tagged $HCN2^{HA_{Ex}}$ ($^{EGFP}HCN2^{HA_{Ex}}$) with VAPB or TM^{VAPB} resulted in increased fluorescence at the plasma membrane **(Fig. 3*A*)**. For these recordings untagged VAPB was used, as fluorescent protein tags have been described to cause a dimerization of VAPB (34, 35). The increased surface expression was quantified detecting HCN2 channels at the cell membrane using non-permeabilized, fixed cells and an ELISA assay, recognizing the extracellular HA-epitope of the $^{EGFP}HCN2^{HA_{Ex}}$ construct. Consistent with the data from the oocyte expression system (Supplemental Fig. 1 and **Fig. 2*F, J*)**, an increased surface expression of HCN2 was observed in the presence of VAPB or TM^{VAPB} **(Fig. 3*B, C*)**. Next, we probed whether the effects of VAPB on HCN2 surface expression are caused by alterations in channel endocytosis. Therefore, we either used dynasore or the C-terminus of the adaptor protein 180 (AP180C), a construct that blocks clathrin-mediated endocytosis (20, 36). Here, despite inhibiting endocytosis by dynasore or AP180C, VAPB increased the HCN2 surface expression with a similar efficiency (Supplemental Fig. 6*A*-*C*). Taken together, these data support that enhanced surface expression of HCN2 is most likely caused by a more efficient forward transport of the channel to the plasma membrane. As HCN2 currents and surface expression are also increased by a minimal VAPB protein (TM^{VAPB}), with a single transmembrane domain **(Fig. 2*H-J*** and **Fig. 3*A, C*)**, the most

straightforward explanation is that VAPB may be part of the native HCN channel complex which is more efficiently transported to the membrane.

Next, we analyzed the endogenous HCN2 expression in primary cortical neurons after transfection with HA-tagged VAPB (^{HA}VAPB) **(Fig. 3*D*)**. Here, HCN2 and transfected ^{HA}VAPB strongly co-localized in the dendrites and the soma of the neurons (merge to white). In contrast, the transfected ALS8 mutation ^{HA}VAPB^{P56S} aggregates in the soma, consistent with previous studies (34) **(Fig. 3*E*)**. Most importantly, HCN2 fluorescence is now primarily located in the soma and a loss of distribution into the dendrites can be observed, albeit the dendrites of the neurons are still intact, as visible from the MAP2 staining of ^{HA}VAPB^{P56S} transfected neurons **(Fig. 3*E*)**.

Co-distribution of VAPs with HCN2 and contribution to thalamic I_h

Furthermore, we investigated the distribution of VAPB, VAPA and HCN2 mRNAs in mouse brain and spinal cord by *in situ* hybridization (ISH) experiments **(Fig. 4*A*-*E*)**. In general, VAPB hybridization signals were weaker than those for VAPA. Highest VAPB mRNA levels were detected in the piriform cortex (Pir) **(Fig. 4*A*)**, the CA3 region of the hippocampus **(Fig. 4*B*)**, the hypothalamic arcuate and ventromedial nucleus and in medial habenulae **(Fig. 4*B, C*)**. An overlapping distribution of VAPB and HCN2 was noted in many brain regions **(*Fig.* 4*A*-*E*)**, particularly evident in the reticular thalamic nucleus (RTh) and globus pallidus **(Fig. 4*C*)**. Hybridization signals for all three transcripts were observed in the subthalamic nucleus (Sth), the ventrobasal thalamic nucleus **(Fig. 4*C*)**, the habenulae **(Fig. 4*B, C*)**, but also the spinal cord **(Fig. 4*E*)**.

While the distribution of VAPB and HCN2 mRNA expression was very similar in all regions examined **(Fig. 4*A*-*E*)**, the VAPA mRNA expression pattern was in some brain regions only partially overlapping. For example, Purkinje cells of the cerebellar cortex express relative high mRNA levels for VAPA, but only very low levels for HCN2 and VAPB **(Fig. 4*D*)**. Most importantly, the observed co-expression of VAPB with HCN2 in the abovementioned neurons is in perfect agreement with the functional interaction we describe.

Consistent with a thalamic co-expression of HCN2 and VAPB and the role of VAPB to increase macroscopic HCN2 and HCN1 currents, patch clamp experiments in neurons of the ventrobasal thalamus of VAPB$^{-/-}$ mice (37) revealed significantly reduced I_h current amplitudes **(Fig. 4*F, G*)**. While I_h current amplitudes were reduced **(Fig. 4*F, G*)**, no major effects on the voltage-dependence of activation were observed **(Fig. 4*H*)**. In addition, we

performed patch clamp experiments of neurons of the piriform cortex which have in contrast to the ventrobasal thalamus a pronounced expression of HCN1 and reduced HCN4 levels (Supplemental Fig. 7*A*-*C* and Material and Methods). Here, we only found a minor reduction of I_h current amplitudes and the voltage-dependence was not significantly altered (Supplemental Fig. 7*D*-*G*). However, the speed of activation was slowed (Supplemental Fig. 7*H*) which is consistent with a reduced relative contribution of HCN1 channel to native I_h currents in the piriform cortex. The fact that kinetics change, while the overall I_h amplitudes largely remain unaltered, indicates that there might be upregulation of other channels or subunits after VAPB knock-out.

Bradycardia in knock-down zebrafish embryos and VAPB$^{-/-}$ mice

In-situ hybridization and RT-PCR experiments using zebrafish hearts at 72 hpf, revealed a cardiac expression of both VAPA and VAPB in the embryonic heart (not illustrated). Using whole-heart immunostainings, VAPB expression was evident throughout the atrium and ventricle of the embryonic zebrafish heart (Supplemental Fig. 8*A*-*B*). Subsequently, to elucidate the functional role of VAPs for cardiac pacemaking *in vivo*, we inactivated either VAPB or VAPA using Morpholino-modified antisense-oligonucleotides (MO), targeting the translation initiation site of zebrafish VAPA (^{MO}VAPA) or VAPB (^{MO}VAPB) **(Fig. 5*A*-*F*)**. Knock-down of either VAPA or VAPB did not cause structural heart defects (data not shown). For ^{MO}VAPB a mild and for ^{MO}VAPA a pronounced pericardial edema was observed **(Fig. 5*A*)**. Moreover, in both types of morphant zebrafish embryos a bradycardia was evident **(Fig. 5*B*)**, with 101 ± 12 bpm for VAPA morphants and 125 ± 10 bpm for ^{MO}VAPB-injected embryos, compared to control-injected embryos with 153 ± 5 bpm. As a proof for the specificity of the knock-down, the heart rate of ^{MO}VAPB-injected embryos could be rescued by the concomitant injection of either VAPA or VAPB cRNA (Supplemental Fig. 8*C*-*D*). Note that the injection of cRNA for the human VAPB^{P56S} mutant into zebrafish embryos did not cause a significant reduction of the heart rate (Supplemental Fig. 8*E*), indicating that the construct does not act in a dominant-negative manner on zebrafish I_f current components. Although heart rate was significantly reduced in VAPA and VAPB morphants, both cardiac chambers, atrium and ventricle, contracted regularly and sequentially as in wild-types, whereby each atrial contraction was followed by a ventricular contraction, indicating unaffected atrio-ventricular conduction. Bradycardia was even more severe when VAPA and VAPB were simultaneously inactivated (^{MO}VAPA/B) and VAPA/VAPB morphants had

severely reduced heart rates (55 ± 41 bpm). In contrast to the VAPA or VAPB morphants, the double knock-down of VAPA and VAPB led to a broad heart rate variability **(Fig. 5*D, E*)** and in 20% of all morphant embryos to severe heart rhythm disturbances (n = 20) **(Fig. 5*F*)**. To evaluate if abnormal cardiac excitation propagation or excitation-contraction-coupling account for bradycardia and heart rhythm disturbance, we monitored free cytosolic myocardial calcium and cardiac contraction simultaneously. In 80% of VAPA/VAPB morphants (n = 20) cardiac excitation starts in the atrium, and propagates from the atrium towards the ventricle, evident as each atrial calcium wave is followed by a calcium wave through the ventricle **(Fig. 5*D, E*)**. In addition, each calcium wave is accompanied by cardiac chamber contraction (not illustrated), indicating that cardiac excitation in VAPA/VAPB morphants is appropriately initiated in the atrium, but with a reduced frequency compared to controls. As described above, in 20% of all ^{MO}VAPA/B-injected embryos conduction abnormalities were observed (n = 20). We found atrio-ventricular blocks, where not every atrial excitation causes ventricular excitation, as evident from **Fig. 5*F*** illustrating a 2:1 atrio-ventricular block. The excitation-contraction coupling of VAPA/VAPB morphants was intact, indicating that knock-down of VAPA/VAPB only impairs the initiation of excitation in the atrium and the atrio-ventricular conduction which is likely to correlate to a QT time prolongation in mice.

Tail-cuff measurements of VAPB$^{-/-}$ mice detected a prominent heart rate reduction **(Fig. 5*G*)** which did however not result in altered blood pressure (Supplemental Fig. 9). Surface ECG recordings of VAPB$^{-/-}$ mice (**Fig. 5*H-N***; and Supplemental Fig. 10 and Supplemental Fig. 11) revealed a sino-atrial bradycardia **(Fig. 5*H, I*)**, as heart rates were reduced while the duration of the PQ interval, corresponding to atrio-ventricular conduction, was unchanged **(Fig. 5*J, K*)**. However, the QTc interval **(Fig. 5*L*)** was prolonged by about 8%. In addition, the T_{peak}-T_{end} (T_p-T_ec) interval **(Fig. 5*M*)** was prolonged and the JT-wave amplitude (JTp) was increased (**Fig. 5*N*** and Supplemental Fig. 11), effects that were also observed for mice with genetically impaired HCN channels (38).

VAPB modulates I_f of spontaneously beating cardiac HL-1 cells

Next, we studied the effects of VAPB in HL-1 cells, a spontaneously beating sino-atrial node like cardiomyocyte cell line (39). HL-1 cells endogenously express VAPB **(Fig. 6*A*)** which was efficiently diminished by shRNA-mediated knock-down **(Fig. 6*B*)**. Overexpression of VAPB in HL-1 cells accelerated spontaneous beating rates **(Fig. 6*E*)**, consistent with

increased I_f amplitudes. As previously reported, not all HL-1 cells express macroscopic I_f currents (27). However, we found 1.5-fold more often I_f-containing cells, when HL-1 cells were transfected with VAPB **(Fig. 6*D*)**. Strikingly, the kinetics of channel activation was accelerated by VAPB **(Fig. 6*C, F*)** and the voltage-dependence of I_f was shifted by +10 mV **(Fig. 6*G, H*)**. This effect can be explained by increased HCN1 and HCN2 current amplitudes and thus a decreased relative contribution of HCN4 to I_f in this cell line. Conversely, shRNA-mediated knock-down of VAPB significantly reduced the spontaneous action potential frequency **(Fig. 6*I, K*)**, by a prolongation of the diastolic depolarization phase **(Fig. 6*I, J*)**. Norepinephrine treatment of HL-1 cells increased the beating frequency and, also under these conditions, VAPB knock-down strongly reduced the beating frequency (Supplemental Fig. *12*). Strikingly, VAPB knock-down had the opposite effects on current kinetics and voltage-dependence, as VAPB overexpression. VAPB knock-down slowed the activation time constants **(Fig. 6*L*)** and led to more hyperpolarized $V_{1/2}$ values (-9 mV) **(Fig. 6*M, N*)**. These *in vitro* data confirm that VAPB serves to increase macroscopic I_f currents in sino-atrial cells, providing an explanation for the sino-atrial bradycardia observed in $VAPB^{-/-}$ mice.

DISCUSSION

As VAPB specifically serves to increase both HCN1 and HCN2 current amplitudes, the knock-out of VAPB results in a similar or even more severe sino-atrial bradycardia than knock-out of the murine HCN1 or HCN2, respectively (40, 41). All HCN isoforms are expressed in the working myocardium (38) and recently an unexpected contribution to the late repolarization phase of the ventricular action potential has been postulated (38, 42, 43). In this case, $HCN3^{-/-}$ mice presented with strong changes in T-wave morphology and a mild (12%) QT-interval prolongation (38). The transmural gradient, with an increased T-wave amplitude, resulted from an action potential duration (APD) shortening selective for epicardial cardiomyocytes. This transmural effect on APD was also present in $HCN1^{-/-}$ mice (38). The mechanism behind this epicardial-specific APD shortening, and why concomitantly a QT-interval prolongation is present, remained elusive. Strikingly, $VAPB^{-/-}$ mice presented a similar phenotype, indicating that VAPB is also an essential component of the ventricular I_f channel complex (38). Thus, in the future, detailed regional action potential studies are indicated in $VAPB^{-/-}$ mice to further investigate this phenomenon. In addition, VAPB might be relevant for inherited forms of ventricular arrhythmias or for arrhythmias in heart failure, where increased ventricular I_f current densities are discussed as a major trigger (43). So far congenital arrhythmias have only been associated with HCN4, the predominant sino-atrial HCN transcript. Possibly human mutations affecting either HCN1 or HCN2 are compensated by the other isoform, preventing a cardiac phenotype. It is conceivable that only a combined reduction of HCN1 and HCN2 current in sino-atrial cells leads to a cardiac phenotype. Similar as for Bartter syndrome Type IV, where the auditory phenotype is only observed when Barttin, the subunit for both ClC-K chloride channels (ClC-Ka and ClC-Kb) is genetically impaired (44), mutations in VAPB might be responsible for cardiac arrhythmias that were not found for HCN1 or HCN2 channels alone.

A major question arising from our results is whether this novel function of VAPB in regulating HCN1 and HCN2 activities could be involved in motor neuron disease. Indeed, gene mutations of *VAPB* have been found in several families developing ALS8, a motor neuron disease also affecting the autonomic nervous system (32, 45), and loss of the VAPB protein occurs in neurons from ALS8 patients (46) as well as in motor neurons of sporadic ALS patients (47). Importantly, the P56S mutation of VAPB leads to a loss of HCN activity **(Fig. 1*T*)**. Thus, mutant VAPB, as well as loss of VAPB, might lower dendritic I_h, primarily encoded by HCN1 and HCN2 in motor neurons (48, 49), thereby decreasing excitability of

motor neurons. Indeed, increasing motor neuron excitability is protective for motor neurons during ALS (50, 51) (reviewed in (52)). Thus, the loss of VAPB in motor neurons, while not sufficient to trigger ALS in mice or zebrafish (37), could substantially contribute to motor neuron degeneration through decreased excitability. On the other hand, the effects might vary by neuron type and brain region. For instance, in the cortex and hippocampus, loss of dendritically-localized I_h is expected to lead to a hyperexcitability.

Arrhythmias and sudden cardiac death (SCD) are common in ALS (53). SCD is responsible for about twenty percent of the death cases in ALS patients (54, 55). ALS patients suffer from prolonged QTc intervals with increased QTc dispersion (54), a dysregulation of the heart rate (56) and have a 25% increased prevalence for atrio-ventricular block (57). However, VAPB mutations are very rare and only one Brazilian family was investigated in depth (58). In this family, there was no evidence of cardiac arrhythmia, and to our knowledge, no patient with a VAPB mutation and typical ALS, as described by Nishimura *et al.* (32), has been studied for cardiac function. On the other hand, as VAPA and VAPB are reduced in ALS patients (34), a dysregulation of HCN channels might be also relevant for sporadic or other familial forms of ALS. The arrhythmias and effects on QTc interval are thought to primarily result from a degeneration of sympathetic neurons of the intermediolateral nucleus (IML) (54). Thus, a reduced sympathetic activity could mask an intrinsic bradycardia, due to a dysregulation of HCN channels. In addition, in ALS patients, afflicted by a severe and life threatening disorder and with the motor symptoms dominating, a bradycardia with less psychological strain might have frequently not been brought to the attention of the physicians.

HCN channels in the brain are modulated by Trip8b (PEX5R) (59) which reduces the cAMP-responsiveness of HCN2 and HCN4 (12), but not of HCN1 channels (60). In addition, however, Trip8b also produces a larger increase in maximal I_h by cAMP (61). The proximal N-terminus of Trip8b is alternatively spliced and differentially controls HCN trafficking and function, with the most prominent neuronal Trip8b isoform enhancing HCN1 channel surface expression (62). This HCN channel modulation is mediated by an interaction with the cyclic-nucleotide binding-domain (63) or the distal C-terminus (59), while the entire C-terminus is dispensable for the interaction of HCN1 and HCN2 with VAPB. Thus, although VAPB and Trip8b both serve to increase surface expression of HCN channels, they act via different binding domains. In addition, VAPB does not cause a modulation of the cAMP-responsiveness of HCN channels. Although the two proteins bind to different regions of the pacemaker channels, it is prompting to analyze whether these subunits act in a synergistic manner or whether there is functional interplay with the Trip8b effects on channel gating.

We conclude that VAPB is an essential regulator of neuronal and cardiac pacemaker channels, modulating the surface expression and cellular localization of HCN2 and HCN1 channels. Therefore, VAPB is likely to play a role in HCN-mediated processes like the regulation of cellular excitability, dendritic integration and transmission of synaptic potentials (64). VAPB modulation of HCN channels might be highly relevant for our understanding of many diseases such as cardiac arrhythmias, epilepsies, inflammatory or neuropathic pain and amyotrophic lateral sclerosis (32, 64).

ACKNOWLEDGMENTS

We thank Oxana Nowak and Andrea Schubert for technical assistance, Nikolaj Klöcker for the $^{EGFP}HCN2^{HA_{Ex}}$ construct and technical advices on the ELISA assays, Caspar Hoogenraad for the ^{HA}VAPB construct, Bernd Fakler for the HCN1 and HCN2 pBF1 constructs and Vijay Renigunta for the HCN4-pBR3-N construct and technical advices on the Y2H screen. We thank Omer Guran for expert help with blinded ECG analysis. L.F. was in part supported by AFNET, European grant agreement No 633196 [CATCH ME], British Heart Foundation (FS/13/43/30324), and the Leducq Foundation. T.B. was supported by a IZKF Münster grant (Bud3/001/016). This work was supported by a grant of the Deutsche Forschungsgemeinschaft (DE 1482/2-1) to N.D..

AUTHOR CONTRIBUTION

TEVC recordings were performed by N. Silbernagel, K.Wemhöner, K.S. Vowinkel and M.A. Komadowski. Macropatch clamp recordings were carried out by M. Schewe, A.K. Kiper and T. Baukrowitz. Patch clamp experiments with iPSC-CMs were performed and supervised by N. Silbernagel and N.D. Ullrich. Patch clamp experiments in HL-1 cells were performed by N. Silbernagel and in HEK293 cells by L.A. Matschke. M. Zobeiri and T. Budde performed slice patch clamp experiments of the piriform cortex and the thalamus. Yeast-experiments were performed by M. Walecki. GST-pull downs were done by N. Silbernagel and S. Rinné. HCN2 surface expression assays were carried out by S. Rinné and N. Silbernagel. Imaging of cortical neurons was performed by N. Silbernagel, A.M. Dolga and L.A. Matschke and of the piriform cortex by M. Zobeiri. N. Silbernagel performed fluorescence imaging experiments. Zebrafish experiments were done by M. Kessler and S. Just. *In situ* hybridization was done by M.K.H. Schäfer, M.A. Komadowski and N. Silbernagel. L. Dupuis and J. Scekic-Zahirovic bred, characterized and provided the $VAPB^{-/-}$ mice. ECG recordings were carried out and analyzed by L. Fortmüller, L. Monassier and L. Fabritz. N. Decher conceived the study. Concept, design and manuscript writing was done by N. Silbernagel and N. Decher. All authors critically read and approved the manuscript.

REFERENCES

1. Biel, M., Schneider, A., and Wahl, C. (2002) Cardiac HCN channels: structure, function, and modulation. *Trends Cardiovasc Med* **12**, 206-212
2. Santoro, B., Liu, D. T., Yao, H., Bartsch, D., Kandel, E. R., Siegelbaum, S. A., and Tibbs, G. R. (1998) Identification of a gene encoding a hyperpolarization-activated pacemaker channel of brain. *Cell* **93**, 717-729
3. DiFrancesco, D. (1993) Pacemaker mechanisms in cardiac tissue. *Annu Rev Physiol* **55**, 455-472
4. Pape, H. C., and McCormick, D. A. (1989) Noradrenaline and serotonin selectively modulate thalamic burst firing by enhancing a hyperpolarization-activated cation current. *Nature* **340**, 715-718
5. Kanyshkova, T., Pawlowski, M., Meuth, P., Dube, C., Bender, R. A., Brewster, A. L., Baumann, A., Baram, T. Z., Pape, H. C., and Budde, T. (2009) Postnatal expression pattern of HCN channel isoforms in thalamic neurons: relationship to maturation of thalamocortical oscillations. *J Neurosci* **29**, 8847-8857
6. Beaumont, V., and Zucker, R. S. (2000) Enhancement of synaptic transmission by cyclic AMP modulation of presynaptic I_h channels. *Nat Neurosci* **3**, 133-141
7. Williams, S. R., and Stuart, G. J. (2000) Site independence of EPSP time course is mediated by dendritic I_h in neocortical pyramidal neurons. *J Neurophysiol* **83**, 3177-3182
8. Ludwig, A., Zong, X., Jeglitsch, M., Hofmann, F., and Biel, M. (1998) A family of hyperpolarization-activated mammalian cation channels. *Nature* **393**, 587-591
9. Zolles, G., Klöcker, N., Wenzel, D., Weisser-Thomas, J., Fleischmann, B. K., Roeper, J., and Fakler, B. (2006) Pacemaking by HCN channels requires interaction with phosphoinositides. *Neuron* **52**, 1027-1036
10. DiFrancesco, D., and Tortora, P. (1991) Direct activation of cardiac pacemaker channels by intracellular cyclic AMP. *Nature* **351**, 145-147
11. Saponaro, A., Pauleta, S. R., Cantini, F., Matzapetakis, M., Hammann, C., Donadoni, C., Hu, L., Thiel, G., Banci, L., Santoro, B., and Moroni, A. (2014) Structural basis for the mutual antagonism of cAMP and TRIP8b in regulating HCN channel function. *Proc Natl Acad Sci U S A* **111**, 14577-14582
12. Zolles, G., Wenzel, D., Bildl, W., Schulte, U., Hofmann, A., Muller, C. S., Thumfart, J. O., Vlachos, A., Deller, T., Pfeifer, A., Fleischmann, B. K., Roeper, J., Fakler, B., and Klöcker, N. (2009) Association with the auxiliary subunit PEX5R/Trip8b controls responsiveness of HCN channels to cAMP and adrenergic stimulation. *Neuron* **62**, 814-825

13. Soussan, L., Burakov, D., Daniels, M. P., Toister-Achituv, M., Porat, A., Yarden, Y., and Elazar, Z. (1999) ERG30, a VAP-33-related protein, functions in protein transport mediated by COPI vesicles. *J Cell Biol* **146**, 301-311
14. Skehel, P. A., Martin, K. C., Kandel, E. R., and Bartsch, D. (1995) A VAMP-binding protein from Aplysia required for neurotransmitter release. *Science* **269**, 1580-1583
15. Foster, L. J., Weir, M. L., Lim, D. Y., Liu, Z., Trimble, W. S., and Klip, A. (2000) A functional role for VAP-33 in insulin-stimulated GLUT4 traffic. *Traffic* **1**, 512-521
16. Lev, S., Ben Halevy, D., Peretti, D., and Dahan, N. (2008) The VAP protein family: from cellular functions to motor neuron disease. *Trends Cell Biol* **18**, 282-290
17. Nishimura, Y., Hayashi, M., Inada, H., and Tanaka, T. (1999) Molecular cloning and characterization of mammalian homologues of vesicle-associated membrane protein-associated (VAMP-associated) proteins. *Biochem Biophys Res Commun* **254**, 21-26
18. Skehel, P. A., Fabian-Fine, R., and Kandel, E. R. (2000) Mouse VAP33 is associated with the endoplasmic reticulum and microtubules. *Proc Natl Acad Sci U S A* **97**, 1101-1106
19. Lvov, A., Chikvashvili, D., Michaelevski, I., and Lotan, I. (2008) VAMP2 interacts directly with the N terminus of Kv2.1 to enhance channel inactivation. *Pflügers Arch* **456**, 1121-1136
20. Renigunta, V., Fischer, T., Zuzarte, M., Kling, S., Zou, X., Siebert, K., Limberg, M. M., Rinné, S., Decher, N., Schlichthörl, G., and Daut, J. (2014) Cooperative endocytosis of the endosomal SNARE protein syntaxin-8 and the potassium channel TASK-1. *Mol Biol Cell* **25**, 1877-1891
21. Friedrich, C., Rinné, S., Zumhagen, S., Kiper, A. K., Silbernagel, N., Netter, M. F., Stallmeyer, B., Schulze-Bahr, E., and Decher, N. (2014) Gain-of-function mutation in TASK-4 channels and severe cardiac conduction disorder. *EMBO Mol Med* **6**, 937-951
22. Dolga, A. M., Terpolilli, N., Kepura, F., Nijholt, I. M., Knaus, H. G., D'Orsi, B., Prehn, J. H., Eisel, U. L., Plant, T., Plesnila, N., and Culmsee, C. (2011) KCa2 channels activation prevents $[Ca^{2+}]_i$ deregulation and reduces neuronal death following glutamate toxicity and cerebral ischemia. *Cell Death Dis* **2**, e147
23. Westerfield, M. (1993) The zebrafish book; a guide for the laboratory use of zebrafish (Brachydanio rerio). *Eugene: University of Oregon Press*
24. Kessler, M., Berger, I. M., Just, S., and Rottbauer, W. (2015) Loss of dihydrolipoyl succinyltransferase (DLST) leads to reduced resting heart rate in the zebrafish. *Basic Res Cardiol* **110**, 14
25. Langenbacher, A. D., Dong, Y., Shu, X., Choi, J., Nicoll, D. A., Goldhaber, J. I., Philipson, K. D., and Chen, J. N. (2005) Mutation in sodium-calcium exchanger 1 (NCX1) causes cardiac fibrillation in zebrafish. *Proc Natl Acad Sci U S A* **102**, 17699-17704

26. Meder, B., Scholz, E. P., Hassel, D., Wolff, C., Just, S., Berger, I. M., Patzel, E., Karle, C., Katus, H. A., and Rottbauer, W. (2011) Reconstitution of defective protein trafficking rescues Long-QT syndrome in zebrafish. *Biochem Biophys Res Commun* **408**, 218-224
27. Sartiani, L., Bochet, P., Cerbai, E., Mugelli, A., and Fischmeister, R. (2002) Functional expression of the hyperpolarization-activated, non-selective cation current I_f in immortalized HL-1 cardiomyocytes. *J Physiol* **545**, 81-92
28. Decher, N., Ortiz-Bonnin, B., Friedrich, C., Schewe, M., Kiper, A. K., Rinné, S., Seemann, G., Peyronnet, R., Zumhagen, S., Bustos, D., Kockskamper, J., Kohl, P., Just, S., Gonzalez, W., Baukrowitz, T., Stallmeyer, B., and Schulze-Bahr, E. (2017) Sodium permeable and "hypersensitive" TREK-1 channels cause ventricular tachycardia. *EMBO Mol Med* **9**, 403-414
29. Johnsson, N., and Varshavsky, A. (1994) Split ubiquitin as a sensor of protein interactions in vivo. *Proc Natl Acad Sci U S A* **91**, 10340-10344
30. Weimbs, T., Low, S. H., Chapin, S. J., Mostov, K. E., Bucher, P., and Hofmann, K. (1997) A conserved domain is present in different families of vesicular fusion proteins: a new superfamily. *Proc Natl Acad Sci U S A* **94**, 3046-3051
31. Weir, M. L., Klip, A., and Trimble, W. S. (1998) Identification of a human homologue of the vesicle-associated membrane protein (VAMP)-associated protein of 33 kDa (VAP-33): a broadly expressed protein that binds to VAMP. *Biochem J* **333 (Pt 2)**, 247-251
32. Nishimura, A. L., Mitne-Neto, M., Silva, H. C., Richieri-Costa, A., Middleton, S., Cascio, D., Kok, F., Oliveira, J. R., Gillingwater, T., Webb, J., Skehel, P., and Zatz, M. (2004) A mutation in the vesicle-trafficking protein VAPB causes late-onset spinal muscular atrophy and amyotrophic lateral sclerosis. *Am J Hum Genet* **75**, 822-831
33. Chen, J., Mitcheson, J. S., Lin, M., and Sanguinetti, M. C. (2000) Functional roles of charged residues in the putative voltage sensor of the HCN2 pacemaker channel. *J Biol Chem* **275**, 36465-36471
34. Teuling, E., Ahmed, S., Haasdijk, E., Demmers, J., Steinmetz, M. O., Akhmanova, A., Jaarsma, D., and Hoogenraad, C. C. (2007) Motor neuron disease-associated mutant vesicle-associated membrane protein-associated protein (VAP) B recruits wild-type VAPs into endoplasmic reticulum-derived tubular aggregates. *J Neurosci* **27**, 9801-9815
35. Gkogkas, C., Middleton, S., Kremer, A. M., Wardrope, C., Hannah, M., Gillingwater, T. H., and Skehel, P. (2008) VAPB interacts with and modulates the activity of ATF6. *Hum Mol Genet* **17**, 1517-1526
36. Doherty, G. J., and McMahon, H. T. (2009) Mechanisms of endocytosis. *Annu Rev Biochem* **78**, 857-902
37. Kabashi, E., El Oussini, H., Bercier, V., Gros-Louis, F., Valdmanis, P. N., McDearmid, J., Mejier, I. A., Dion, P. A., Dupre, N., Hollinger, D., Sinniger, J., Dirrig-Grosch, S., Camu, W., Meininger, V., Loeffler, J. P., Rene, F., Drapeau, P., Rouleau, G. A., and Dupuis, L. (2013)

Investigating the contribution of VAPB/ALS8 loss of function in amyotrophic lateral sclerosis. *Hum Mol Genet* **22**, 2350-2360

38. Fenske, S., Mader, R., Scharr, A., Paparizos, C., Cao-Ehlker, X., Michalakis, S., Shaltiel, L., Weidinger, M., Stieber, J., Feil, S., Feil, R., Hofmann, F., Wahl-Schott, C., and Biel, M. (2011) HCN3 contributes to the ventricular action potential waveform in the murine heart. *Circ Res* **109**, 1015-1023
39. Claycomb, W. C., Lanson, N. A., Jr., Stallworth, B. S., Egeland, D. B., Delcarpio, J. B., Bahinski, A., and Izzo, N. J., Jr. (1998) HL-1 cells: a cardiac muscle cell line that contracts and retains phenotypic characteristics of the adult cardiomyocyte. *Proc Natl Acad Sci U S A* **95**, 2979-2984
40. Fenske, S., Krause, S. C., Hassan, S. I., Becirovic, E., Auer, F., Bernard, R., Kupatt, C., Lange, P., Ziegler, T., Wotjak, C. T., Zhang, H., Hammelmann, V., Paparizos, C., Biel, M., and Wahl-Schott, C. A. (2013) Sick sinus syndrome in HCN1-deficient mice. *Circulation* **128**, 2585-2594
41. Ludwig, A., Budde, T., Stieber, J., Moosmang, S., Wahl, C., Holthoff, K., Langebartels, A., Wotjak, C., Munsch, T., Zong, X., Feil, S., Feil, R., Lancel, M., Chien, K. R., Konnerth, A., Pape, H. C., Biel, M., and Hofmann, F. (2003) Absence epilepsy and sinus dysrhythmia in mice lacking the pacemaker channel HCN2. *EMBO J* **22**, 216-224
42. Fenske, S., Krause, S., Biel, M., and Wahl-Schott, C. (2011) The role of HCN channels in ventricular repolarization. *Trends Cardiovasc Med* **21**, 216-220
43. Hofmann, F., Fabritz, L., Stieber, J., Schmitt, J., Kirchhof, P., Ludwig, A., and Herrmann, S. (2012) Ventricular HCN channels decrease the repolarization reserve in the hypertrophic heart. *Cardiovasc Res* **95**, 317-326
44. Estevez, R., Boettger, T., Stein, V., Birkenhager, R., Otto, E., Hildebrandt, F., and Jentsch, T. J. (2001) Barttin is a Cl^- channel beta-subunit crucial for renal Cl^- reabsorption and inner ear K^+ secretion. *Nature* **414**, 558-561
45. Marques, V. D., and Marques, W., Jr. (2008) Neurophysiological findings of the late-onset, dominant, proximal spinal muscular atrophies with dysautonomia because of the VAPB PRO56SER mutation. *J Clin Neurophysiol* **25**, 233-235
46. Mitne-Neto, M., Machado-Costa, M., Marchetto, M. C., Bengtson, M. H., Joazeiro, C. A., Tsuda, H., Bellen, H. J., Silva, H. C., Oliveira, A. S., Lazar, M., Muotri, A. R., and Zatz, M. (2011) Downregulation of VAPB expression in motor neurons derived from induced pluripotent stem cells of ALS8 patients. *Hum Mol Genet* **20**, 3642-3652
47. Anagnostou, G., Akbar, M. T., Paul, P., Angelinetta, C., Steiner, T. J., and de Belleroche, J. (2010) Vesicle associated membrane protein B (VAPB) is decreased in ALS spinal cord. *Neurobiol Aging* **31**, 969-985

48. Pape, H. C. (1996) Queer current and pacemaker: the hyperpolarization-activated cation current in neurons. *Annu Rev Physiol* **58**, 299-327
49. Chen, X., Sirois, J. E., Lei, Q., Talley, E. M., Lynch, C., 3rd, and Bayliss, D. A. (2005) HCN subunit-specific and cAMP-modulated effects of anesthetics on neuronal pacemaker currents. *J Neurosci* **25**, 5803-5814
50. Saxena, S., Roselli, F., Singh, K., Leptien, K., Julien, J. P., Gros-Louis, F., and Caroni, P. (2013) Neuroprotection through excitability and mTOR required in ALS motoneurons to delay disease and extend survival. *Neuron* **80**, 80-96
51. Leroy, F., Lamotte d'Incamps, B., Imhoff-Manuel, R. D., and Zytnicki, D. (2014) Early intrinsic hyperexcitability does not contribute to motoneuron degeneration in amyotrophic lateral sclerosis. *Elife* **3**
52. Roselli, F., and Caroni, P. (2015) From intrinsic firing properties to selective neuronal vulnerability in neurodegenerative diseases. *Neuron* **85**, 901-910
53. Finsterer, J., Stollberger, C., and Maeztu, C. (2016) Sudden cardiac death in neuromuscular disorders. *Int J Cardiol* **203**, 508-515
54. Asai, H., Hirano, M., Udaka, F., Shimada, K., Oda, M., Kubori, T., Nishinaka, K., Tsujimura, T., Izumi, Y., Konishi, N., Matsumoto, S., Kameyama, M., and Ueno, S. (2007) Sympathetic disturbances increase risk of sudden cardiac arrest in sporadic ALS. *J Neurol Sci* **254**, 78-83
55. Shimizu, T., Hayashi, H., Kato, S., Hayashi, M., Tanabe, H., and Oda, M. (1994) Circulatory collapse and sudden death in respirator-dependent amyotrophic lateral sclerosis. *J Neurol Sci* **124**, 45-55
56. Murata, Y., Harada, T., Ishizaki, F., Izumi, Y., and Nakamura, S. (1997) An abnormal relationship between blood pressure and pulse rate in amyotrophic lateral sclerosis. *Acta Neurol Scand* **96**, 118-122
57. Shemisa, K., Kaelber, D., Parikh, S. A., and Mackall, J. A. (2014) Autonomic etiology of heart block in amyotrophic lateral sclerosis: a case report. *J Med Case Rep* **8**, 224
58. Marques, V. D., Barreira, A. A., Davis, M. B., Abou-Sleiman, P. M., Silva, W. A., Jr., Zago, M. A., Sobreira, C., Fazan, V., and Marques, W., Jr. (2006) Expanding the phenotypes of the Pro56Ser VAPB mutation: proximal SMA with dysautonomia. *Muscle Nerve* **34**, 731-739
59. Santoro, B., Wainger, B. J., and Siegelbaum, S. A. (2004) Regulation of HCN channel surface expression by a novel C-terminal protein-protein interaction. *J Neurosci* **24**, 10750-10762
60. Santoro, B., Piskorowski, R. A., Pian, P., Hu, L., Liu, H., and Siegelbaum, S. A. (2009) TRIP8b splice variants form a family of auxiliary subunits that regulate gating and trafficking of HCN channels in the brain. *Neuron* **62**, 802-813
61. Hu, L., Santoro, B., Saponaro, A., Liu, H., Moroni, A., and Siegelbaum, S. (2013) Binding of the auxiliary subunit TRIP8b to HCN channels shifts the mode of action of cAMP. *J Gen Physiol* **142**, 599-612

62. Lewis, A. S., Schwartz, E., Chan, C. S., Noam, Y., Shin, M., Wadman, W. J., Surmeier, D. J., Baram, T. Z., Macdonald, R. L., and Chetkovich, D. M. (2009) Alternatively spliced isoforms of TRIP8b differentially control h channel trafficking and function. *J Neurosci* **29**, 6250-6265

63. Han, Y., Noam, Y., Lewis, A. S., Gallagher, J. J., Wadman, W. J., Baram, T. Z., and Chetkovich, D. M. (2011) Trafficking and gating of hyperpolarization-activated cyclic nucleotide-gated channels are regulated by interaction with tetratricopeptide repeat-containing Rab8b-interacting protein (TRIP8b) and cyclic AMP at distinct sites. *J Biol Chem* **286**, 20823-20834

64. DiFrancesco, J. C., and DiFrancesco, D. (2015) Dysfunctional HCN ion channels in neurological diseases. *Front Cell Neurosci* **6**, 174

FIGURE LEGENDS

Figure 1. VAPB selectively increases HCN1 and HCN2 currents. *A*) Y2H direct interaction assay. Transformation control (-LW), leucine and tryptophan dropout. Interaction read-out (-LWHA), additional dropout of histidine and adenine. pAL-Alg5, positive control. pPR3-N, negative control. *B*) Topology of VAPB. MSP, major sperm protein domain; CC, coiled-coil domain; TM, transmembrane segment. *C*) ^{GST}VAPB pull-down of HCN2^{EGFP} using transfected HeLa cells. *D*) ^{GST}VAPA, ^{GST}VAMP1 or ^{GST}VAMP2 pull-down of HCN2^{EGFP} using transfected HeLa cells. *E*) ^{GST}VAPA pull-down of HCN2 and endogenous VAPB, using HCN2^{EGFP} transfected HeLa cells. *F*) Pull-down of *in vitro* translated HCN2 (untagged). *G*) Pull-down of HCN2 from rat brain lysates. *H*) Representative currents of HCN2 expressed in oocytes alone or with VAPB and *I*) the relative current amplitudes analyzed over three days. *J*) Relative currents of HCN1, HCN2 and HCN4 alone or co-expressed with VAPB. *K*) Relative currents of different potassium channels co-expressed with VAPB and of *L*) HCN2 co-expressed with VAPA, VAPB or VAPC. *M*) Relative currents of HCN2 co-expressed with a mixture of VAPA/B (1:1). *N*) Representative macropatch recordings in different configurations: on cell (o.c.), inside-out after patch excision (i.o.) and after application of 100 µM cAMP (i.o.+100 µM cAMP). *O*) Activation curves for HCN2 alone (n = 6) recorded as in *N*) or *P*) after co-expression with VAPB (n = 8). *Q*) $V_{1/2}$ values for HCN2 expressed alone or with VAPB in different patch modes. *R*) Relative currents of HCN2$^{HA_{Ex}}$ alone or with VAPB. *S*) Relative surface expression of HCN2$^{HA_{Ex}}$ expressed alone or with VAPB, analyzed as Relative Light Units (RLUs). *T*) Relative currents of HCN2 expressed alone or with VAPB or VAPB^{P56S}. All data are presented as mean ± s.e.m.. The number of cells (n) are indicated in the bar graphs. *, $P < 0.05$; **; $P < 0.01$; ***, $P < 0.001$ using an unpaired Student´s T-test, except for panels *I*), *J*), *N*), *M*) and *T*) using a Mann-Whitney-U-test.

Figure 2. Domains mediating the interaction of VAPB with HCN2. *A*) Schematic illustration of a HCN subunit. The cyclic-nucleotide binding-domain (CNBD) and some of the truncation constructs studied are indicated. *B*) All truncation constructs showed a positive interaction, evident from growth on -LWHA drop out medium. *C*) Representative current traces and the relative currents for different C-terminal deletions expressed alone or with VAPB. *D*) Representative current traces and the relative current amplitudes for the N-terminal truncated ^{NTK}HCN2 expressed alone or with VAPB. *E*) Relative current amplitudes of ^{NTK}HCN2$^{HA_{Ex}}$ (extracellular HA-tag) expressed alone or with VAPB. *F*) Relative surface expression of

^{NTK}HCN2$^{HA_{Ex}}$ expressed alone or with VAPB analyzed as Relative Light Units (RLUs). *G*) Schematic illustration, representative traces and currents of a HCN2 channel chimera with the N-terminus of HCN4 ($^{HCN4\text{-}N}$HCN2) expressed alone or with VAPB. *H*) Relative currents of HCN2 expressed alone or co-expressed with VAPB (1.7 ± 0.1), TM^{VAPB} (1.6 ± 0.2), the major sperm domain (MSP^{VAPB}), the MSP with half of the coiled-coil (CC) domain (MSP-CC$_{0.5}$^{VAPB}) or with the complete CC domain (MSP-CC^{VAPB}). *I*) Relative current amplitudes of HCN2$^{HA_{Ex}}$ expressed alone or with TM^{VAPB} (1.3 ± 0.1) and *J*) the respective changes in the relative surface membrane expression analyzed as RLUs, using a single cell chemiluminescence assay (TM^{VAPB} 1.8 ± 0.2). All data are presented as mean ± s.e.m.. The number of experiments (*n*) are indicated in the respective bar graphs. *, P < 0.05; **, P < 0.01; ***, P < 0.001 using an unpaired Student´s T-test, except for panels *C*), *D*), *F*), *G*), *H*) and *J*) using a Mann-Whitney-U-test and for panel i using Welch's T-test.

Figure 3. VAPB determines surface expression and dendritic localization of HCN2. *A*) Live cell imaging of HeLa cells transfected with a N-terminally EGFP-tagged HCN2 carrying an extracellular HA-epitope (^{EGFP}HCN2$^{HA_{Ex}}$) alone or co-transfected with VAPB or the transmembrane segment of VAPB (TM^{VAPB}). *B*) Chemiluminescence assays of fixed non-permeabilized HeLa cells, analyzing the surface expression as Relative Light Units (RLUs) for ^{EGFP}HCN2$^{HA_{Ex}}$ alone and after co-transfection with VAPB (1.6 ± 0.1). Upper inset illustrates a representative control Western blot showing an unaltered HCN2 protein expression. *C*) Chemiluminescence surface expression assay as in *B*), but using TM^{VAPB} (1.6 ± 0.1). *D*) Immunocytochemistry of ^{HA}VAPB transfected cortical neurons. Endogenous HCN2 (green) is co-localizing (white) with ^{HA}VAPB (magenta) in the soma and dendrites. Anti MAP2-staining illustrating an intact neuronal network and dendrites (blue). *E*) Immunocytochemistry experiment as in d, but transfecting the ALS8 mutation ^{HA}VAPB^{P56S} (magenta), leading to an aggregation of VAPB^{P56S} in the soma of the neurons. Also HCN2 fluorescence (green) was focused in the soma and dendritic localization was lost, despite an intact neuronal network (α-MAP2, blue). All data are presented as mean ± s.e.m.. The number of experiments (*n*) are indicated in the respective bar graphs. **; P < 0.01 using an unpaired Student´s T-test. Scale bars for *A*), *D*) and *E*), 20 µm.

Figure 4. Co-distribution of VAPs with HCN2 and contribution to thalamic I_h. *A*)-*E*), Distribution of HCN2, VAPB and VAPA mRNA in mouse brain and spinal cord. *In situ* hybridization analysis of HCN2, VAPB and VAPA using digoxigenin-labeled riboprobes,

revealing mRNA expression of VAPB in *A*) cortical areas *B*) hippocampus *C*) thalamus *D*) cerebellum (arrows point to interneurons in the granular layer) and *E*) spinal cord. Note the overlapping distribution of VAPB with HCN2 and VAPA mRNA. Pir, piriform cortex; Am, amygdala; ic, internal capsule; Th, thalamus; CA, cornu ammonis; DG, dentate gyrus; LG, lateral geniculate ncl.; VB, ventrobasal thalamus; RTh, reticular thalamic ncl.; Sth, subthalamic ncl.; Hb, habenulae; gcl, granule cell layer; pcl, purkinje cell layer; m, molecular cell layer; DH, dorsal horn; VH, ventral horn. *F*) Representative current traces elicited in slice patch clamp experiments of the ventrobasal thalamus (VB) of wild-type animals (control) and $VAPB^{-/-}$ mice. *G*) The I_h current was significantly reduced in $VAPB^{-/-}$ mice (15.4 ± 1.1 pA/pF) compared to control animals (22.2 ± 2.3 pA/pF). *H*) Average activation curves of the VB I_h current for control and $VAPB^{-/-}$ mice. $V_{1/2}$ of activation for control (-91.6 ±1.3 mV, n = 8) and $VAPB^{-/-}$ (-87.5 ± 1.2 mV, n = 7). All data are presented as mean ± s.e.m.. The number of experiments (*n*) are indicated in the respective bar graphs. *, $P < 0.05$ using an unpaired Student´s T-test. Scale bars, 500 µm, except for *D*), 100 µm.

Figure 5. Bradycardia in knock-down zebrafish embryos and $VAPB^{-/-}$ mice. *A*) Zebrafish embryos at 72 hours post fertilization (hpf). Control-injected and Morpholino-antisense (MO) injected embryos against VAPA (^{MO}VAPA) or VAPB (^{MO}VAPB) exhibit no significant abnormalities (left), in particular no structural heart defects (right). Note a light cardiac edema in ^{MO}VAPB and a strong edema in ^{MO}VAPA. *B*) Heart rate in beats per minute (bpm) of control and ^{MO}VAPA, ^{MO}VAPB or ^{MO}VAPA/B injected zebrafish embryos at 72 hpf. *C*) Representative examples of calcium transients (relative fluorescence intensity) in the cardiac atrium (black) and cardiac ventricle (gray) of control-injected zebrafish at 72 hpf, displaying a regular atrio-ventricular propagation of excitation from atrium to ventricle in a 1:1-ratio. *D*)-F), Representative calcium transients recorded in ^{MO}VAPA/B double knock-down morphants, illustrating *D*) and *E*) strongly reduced heart rates with variable frequency. *F*) Representative example of atrial and ventricular calcium measurements from a ^{MO}VAPA/B morphant with a 2:1 atrio-ventricular block, where only every second atrial excitation leads to a ventricular excitation. *A*)-*F*), Data were obtained from three independent batches of injections. *G*) Heart rate in beats per minute (bpm) of $VAPB^{-/-}$ mice compared to wild-type littermates (control), analyzed by tail-cuff measurements. *H*) Representative surface electrocardiogram (ECG) recordings of $VAPB^{-/-}$ mice and their wild-type littermates (control). ECG of $VAPB^{-/-}$ mice show bradycardia and an increased T-wave amplitude. *I*)-*N*), Analyses of the ECG parameters of $VAPB^{-/-}$ mice. *I*), Heart rate in beats per minute (bpm). *J*) PQ interval (PQ) duration. *K*)

QRS complex (QRS) duration. *L*) Frequency corrected QT interval (QTc). *M*) Frequency corrected T_{peak} to T_{end} duration (T_p-T_ec). *N*) T-wave amplitude (JT_p). All data are presented as mean ± s.e.m.. The number of animals (*n*) is indicated in the respective bar graphs. *, $P < 0.05$; **, $P < 0.01$; ***, $P < 0.001$ using an unpaired Student´s T-test, except for panels *B*) and *I*) using Welch's T-test. Scale bars for *A*), 500 µm, for *C*)-*F*), 500 ms and for *H*), 100 ms.

Figure 6. VAPB modulates I_f of spontaneously beating cardiac HL-1 cells. *A*) Immunocytochemistry of VAPB in HL-1 cells. *B*) Western blot illustrating the knock-down of VAPB expression in HL-1 cells by shRNA transfection. Control, HL-1 cells transfected with scrambled shRNA. *C*) Representative I_f currents of HL-1 cells under control conditions and after VAPB transfection. *D*) Percentage of HL-1 cells containing I_f under control conditions (38%) and after VAPB transfection (58%). *E*) Beating frequency under control conditions (158 ± 4) and after VAPB transfection (179 ± 4), analyzed by optical counting of contractions in original Claycomb medium containing norepinephrine (60). *F*) Accelerated activation kinetics of VAPB transfected HL-1 cells (n = 9 - 10). *G*) Activation curves of HL-1 cells under control conditions (n = 10) and after VAPB transfection (n = 11). *H*) Positive shift in the $V_{1/2}$ of activation of I_f recorded in VAPB transfected HL-1 cells. Control (scrambled shRNA), -90.3 ± 3.4 mV (n = 10); VAPB transfected, -79.6 ± 2.7 mV (n = 11). *I*) Representative action potential measurements of wild-type HL-1 and shRNA transfected cells (shVAPB). *J*) Analysis of the diastolic depolarization (DD duration). *K*) Beating frequency of HL-1 cells under control conditions and after VAPB knock-down. *L*) VAPB knock-down slows the activation kinetics (n = 5) of endogenous I_f currents. *M*) Transfection of shRNA (n = 5) shifts the voltage-dependence of activation ($V_{1/2}$) of I_f to more negative potentials (n = 6). *N*) $V_{1/2}$ values for control (scrambled shRNA) were -88.2 ± 3.1 mV (n = 6) and for shRNA-transfection (shVAPB) -96.2 ± 2.3 mV (n = 5), respectively. *I*)-*J*), Scrambled shRNA was used as control. All data are presented as mean ± s.e.m.. The number of experiments (*n*) are indicated in the bar graphs. *, $P < 0.05$; **, $P < 0.01$; ***, $P < 0.001$ using an unpaired Student´s T-test, except for panels *E*), *F*), *J*), *K*), *L*) and *N*) using a Mann-Whitney-U-test. Scale bars for *A*), 20 µm.

Figures

Figure 1

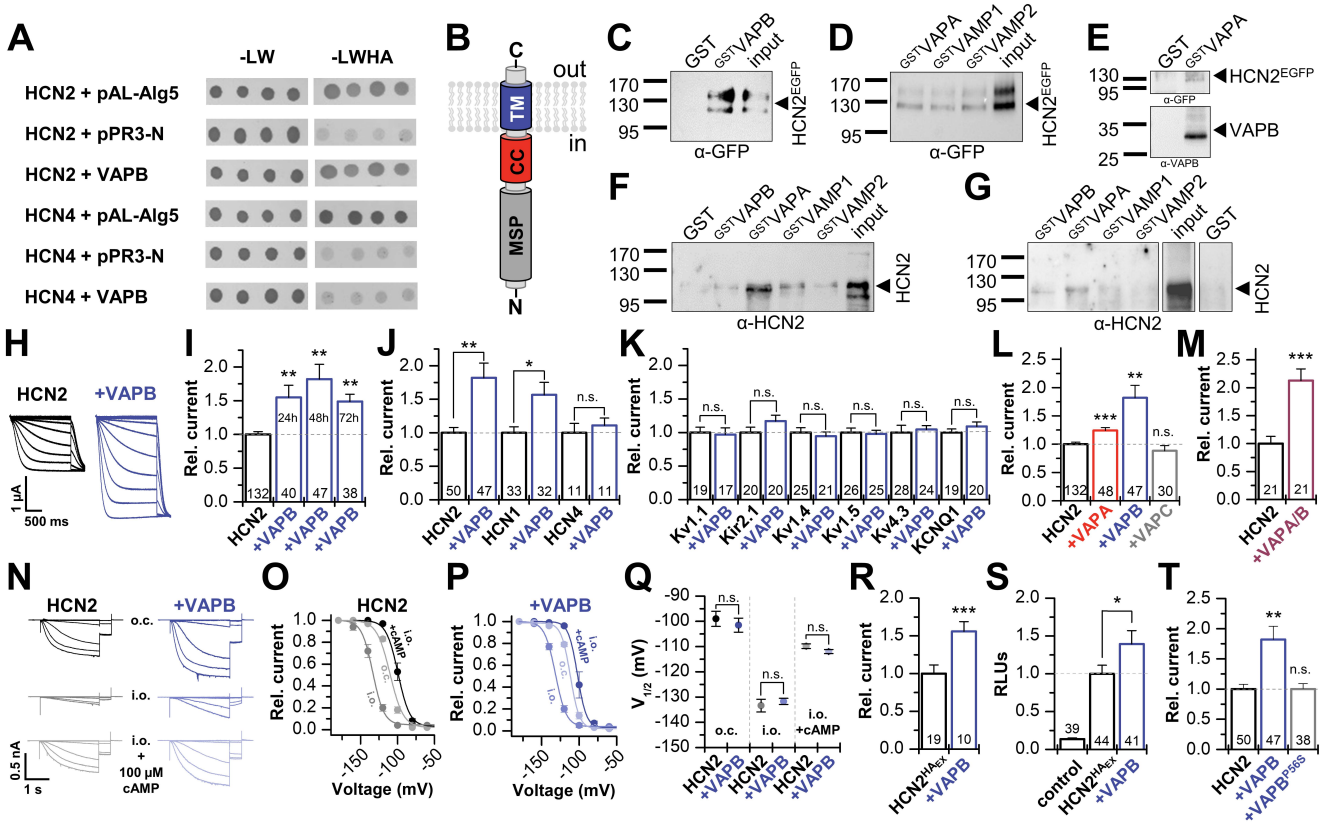

Figure 2

Figures

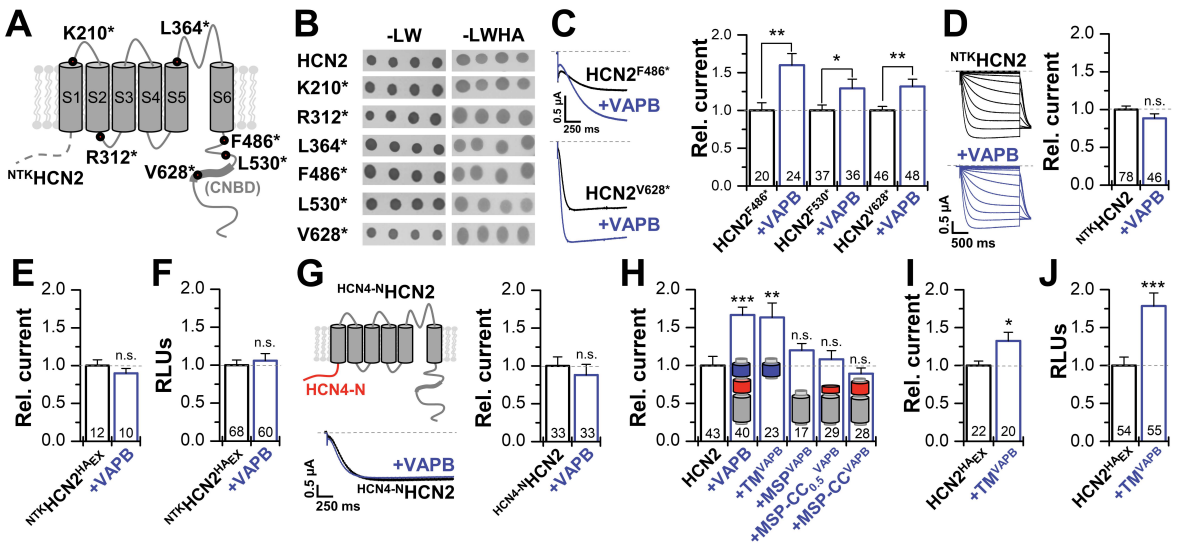

Figure 3

Figures

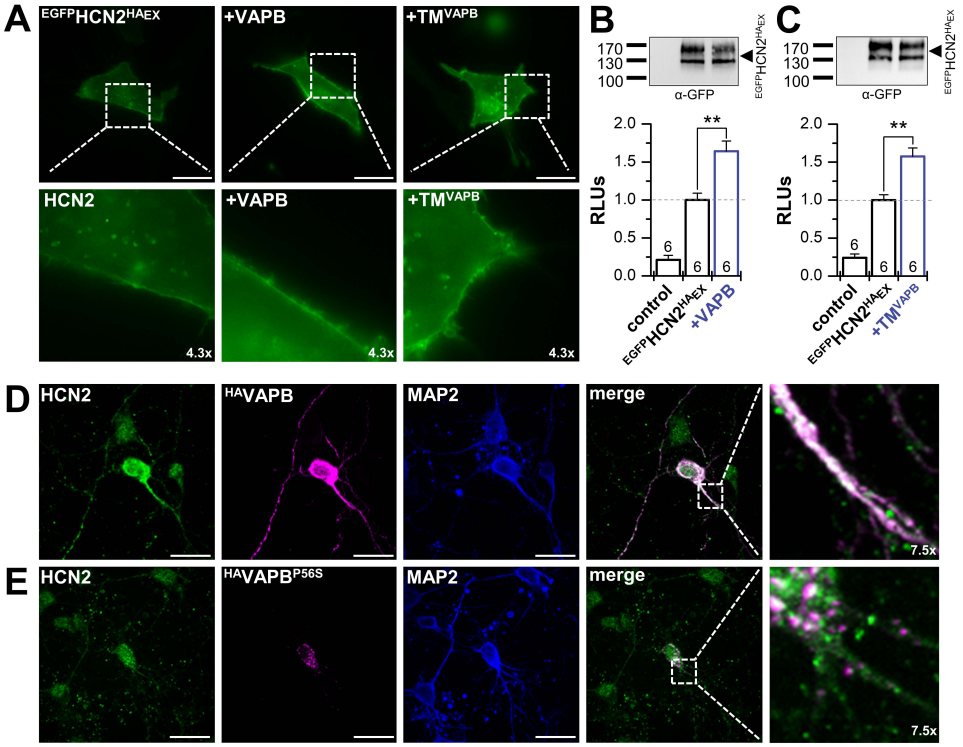

Figures

Figure 4

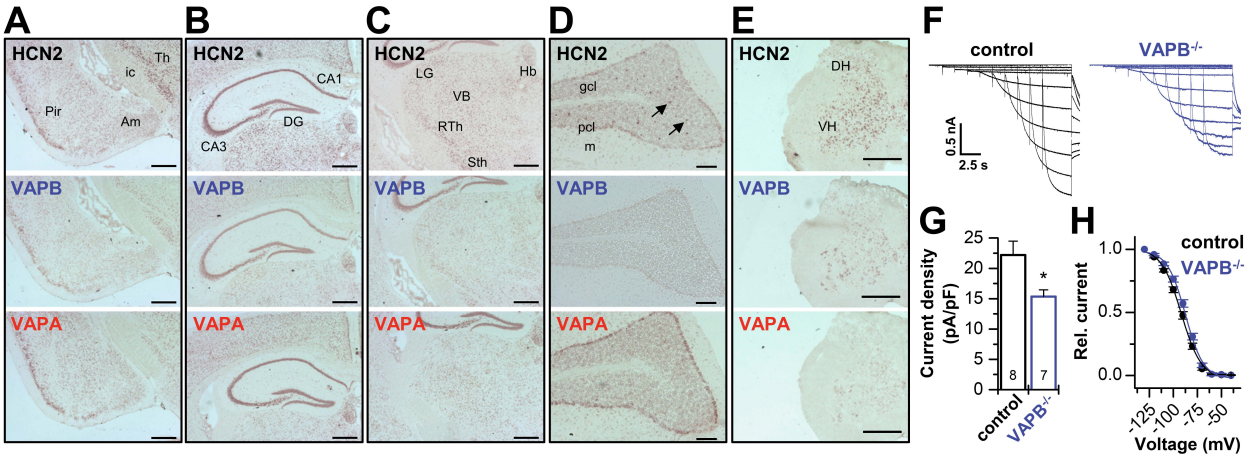

Figure 5

Figures

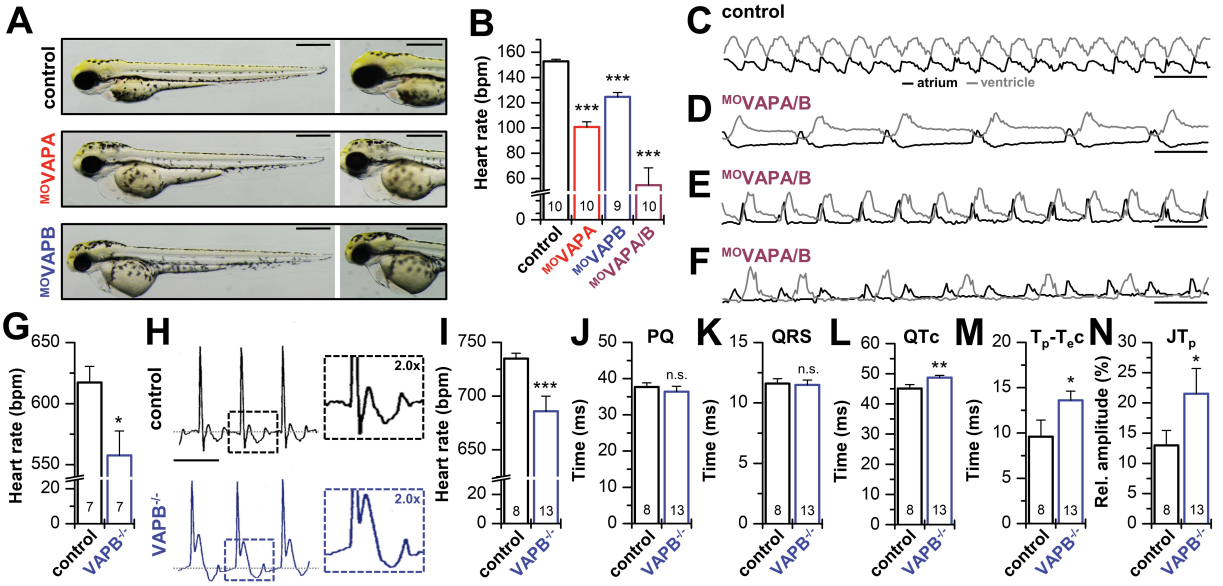

Figure 6

Figures